Monthly Notices
of the
ROYAL ASTRONOMICAL SOCIETY

MNRAS **489,** 2488–2504 (2019)
Advance Access publication 2019 July 30

doi:10.1093/mnras/stz2082

The complete local volume groups sample – III. Characteristics of group central radio galaxies in the Local Universe

Konstantinos Kolokythas,[1]★ Ewan O'Sullivan,[2] Huib Intema,[3,4] Somak Raychaudhury,[1,5,6] Arif Babul,[7,8] Simona Giacintucci[9] and Myriam Gitti[10,11]

[1]*Inter-University Centre for Astronomy and Astrophysics, Pune University Campus, Ganeshkhind, Pune, Maharashtra 411007, India*
[2]*Harvard-Smithsonian Center for Astrophysics, 60 Garden Street, Cambridge, MA 02138, USA*
[3]*International Centre for Radio Astronomy Research, Curtin University, Bentley, WA 6102, Australia*
[4]*Leiden Observatory, Leiden University, Niels Bohrweg 2, 2333 CA Leiden, the Netherlands*
[5]*School of Physics and Astronomy, University of Birmingham, Birmingham B15 2TT, UK*
[6]*Department of Physics, Presidency University, 86/1 College Street, Kolkata 700073, India*
[7]*Department of Physics and Astronomy, University of Victoria, Victoria, BC V8P 1A1, Canada*
[8]*Center for Theoretical Astrophysics and Cosmology, Institute for Computational Science, University of Zurich, Winterthurerstrasse 190, 8057 Zurich, Switzerland*
[9]*Naval Research Laboratory, 4555 Overlook Avenue SW, Code 7213, Washington, DC 20375, USA*
[10]*Dipartimento di Fisica e Astronomia, Universitá di Bologna, via Gobetti 93/2, 40129 Bologna, Italy*
[11]*INAF, Istituto di Radioastronomia di Bologna, via Gobetti 101, 40129 Bologna, Italy*

Accepted 2019 July 22. Received 2019 July 17; in original form 2019 May 31

ABSTRACT

Using new 610 and 235 MHz observations from the giant metrewave radio telescope (GMRT) in combination with archival GMRT and very large array (VLA) survey data, we present the radio properties of the dominant early-type galaxies in the low-richness subsample of the complete local-volume groups sample (CLoGS; 27 galaxy groups) and provide results for the radio properties of the full CLoGS sample for the first time. We find a high radio detection rate in the dominant galaxies of the low-richness subsample of 82 per cent (22/27); for the full CLoGS sample the detection rate is 87 per cent (46/53). The group-dominant galaxies exhibit a wide range of radio power, 10^{20}–10^{25} W Hz^{-1} in the 235 and 610 MHz bands, with the majority (53 per cent) presenting point-like radio emission, 19 per cent hosting currently active radio jets, 6 per cent having remnant jets, 9 per cent being diffuse, and 13 per cent having no detected radio emission. The mean spectral index of the detected radio sources in the 235−610 MHz frequency range is found to be $\alpha_{235}^{610} \sim 0.68$, and $\alpha_{235}^{1400} \sim 0.59$ in the 235−1400 MHz one. In agreement with earlier studies, we find that the fraction of ultrasteep spectrum sources ($\alpha > 1.3$) is ∼4 per cent, mostly dependent on the detection limit at 235 MHz. The majority of point-like systems are found to reside in dynamically young groups, whereas jet systems show no preference between spiral-rich and spiral-poor group environments. The mechanical power of the jet sources in the low-richness sample groups is estimated to be $\sim 10^{42}$–10^{44} erg s^{-1} with their black hole masses ranging between 2×10^8 and 5×10^9 M$_\odot$. We confirm previous findings that while radio jet sources tend to be associated with more massive black holes, black hole mass is not the decisive factor in determining jet activity or power.

Key words: galaxies: active – galaxies: groups: general – galaxies: jets – radio continuum: galaxies.

1 INTRODUCTION

The bulk of galaxies and baryonic matter in the local Universe is found in galaxy groups (Geller & Huchra 1983; Fukugita, Hogan & Peebles 1998; Eke et al. 2005). Typically, they extend less than a Mpc with a mass range of $10^{12.5}$–10^{14} M$_\odot$ (Huchra & Geller 1983), about an order of magnitude less massive than galaxy clusters. Galaxy groups exhibit shallow gravitational potential wells, with their members being at close distances and at low relative velocities. These parameters are essential in driving the transformation processes (e.g. mergers and tidal interactions) of

★ E-mail: kkolok@iucaa.in

galaxy evolution (e.g. Alonso et al. 2012). Galaxies are thought to be 'pre-processed' in the group environment before they become parts of clusters (e.g. van den Bosch et al. 2014; Haines et al. 2018), hence the association between rich cluster galaxies and their evolution is intimately linked to the group environment (e.g. Bekki, Shioya & Tanaka 1999; Moss & Whittle 2000). Since the properties of galaxies and their evolution depends on their local environment, galaxy groups are an ideal environment where the study of galaxy formation and evolution is of uttermost significance (e.g. Forbes et al. 2006; Sun 2012).

Many groups maintain extensive haloes of hot gas with short central cooling times (e.g. O'Sullivan et al. 2017), which can fuel both star formation and active galactic nuclei (AGN). However, the cool gas can either be removed from the central region via AGN outflows (Alexander et al. 2010; Morganti et al. 2013) or heated up, eventually suppressing star formation and galaxy growth. The imprints of such a heating mechanism ('feedback') capable of balancing the radiative losses in central dominant early-type galaxies are evident via the interaction of radio-loud AGN activity and the surrounding hot X-ray gas, leading to excavation of cavities (e.g. McNamara et al. 2005; McNamara & Nulsen 2007). Their low masses mean that galaxy groups are the environment in which AGN feedback mechanism may have the greatest impact on the evolution of the hot diffuse gas.

It has been suggested that in most groups and clusters, feedback operates in a near-continuous 'bubbling' mode where thermal regulation is relatively gentle (Bîrzan et al. 2008, 2012; Panagoulia et al. 2014). However, there are cases that AGN feedback can also manifest via extreme AGN outbursts, potentially shutting down the central engine for long periods (e.g. in Hydra A, MS 0735 + 7421, NGC 4261, NGC 193 & IC 4296; Rafferty et al. 2006; Gitti et al. 2007; O'Sullivan et al. 2011; Gitti, Brighenti & McNamara 2012; Kolokythas et al. 2015, 2018; Grossova et al. 2019). Such powerful outbursts may have a significant effect on the development of groups, and it is therefore vital to study the energy output of radio galaxies in an unbiased set of low-mass systems in order to understand the impact of AGN in the group regime.

It is well known that galaxies at the centres of evolved groups are generally early types, lacking strong ongoing star formation (e.g. Vaddi et al. 2016), with their properties depending strongly on the group halo mass (De Lucia & Blaizot 2007; Skibba & Sheth 2009; Gozaliasl et al. 2018), and the galaxy density (i.e. compact versus loose groups). Brightest group early-type galaxies (BGEs) as well as brightest cluster galaxies (BCGs), exhibit different surface brightness profiles and scaling relations from field or satellite massive galaxies (e.g. Graham et al. 1996; Bernardi et al. 2007) and play an important role in the evolution of galaxy groups. They are also found to exhibit different morphologies, star formation rates, radio emission, and AGN properties compared to satellite galaxies of the same stellar mass. Their privileged position near or at the centres of the extended X-ray emitting hot intragroup medium (IGM) and dark matter halo makes them suitable laboratories for constraining cosmological models, for studying the growth history of massive galaxies (e.g. von der Linden et al. 2007; Liu et al. 2009; Stott et al. 2010; Liang et al. 2016), their supermassive black holes (e.g. Rafferty et al. 2006; Sabater et al. 2019), and the connection between galaxy properties such as stellar kinematics and the larger environment (Loubser et al. 2018).

The radio detection rate of massive galaxies is found to be ∼30 per cent (e.g. Best et al. 2005; Shabala et al. 2008), but this is dependent on the sensitivity of the survey used and the redshift range considered. Studies of the BGEs/BCGS of groups and clusters in the local Universe finding shows detection rates of ∼80−90 per cent (e.g. Magliocchetti & Brüggen 2007; Dunn et al. ; Kolokythas et al. 2018) and this can even rise to 100 per cent for the most massive systems (Sabater et al. 2019). It has been suggested that, in addition to fuelling of AGN by cooling from the IGM, the connection between radio AGN and higher galaxy densities (Lilly et al. 2009; Bardelli et al. 2010; Malavasi et al. 2015) may be driven by large-scale merging (e.g. infall of groups into clusters) or by 'intergroup' galaxy–galaxy interactions and mergers (Miles et al. 2004; Taylor & Babul 2005). In such mergers and interactions gas can be channelled to the central AGN resulting in radio emission and the launching of jets. However, although AGNs dominate the radio emission from these massive galaxies, star formation may contribute in the less radio luminous objects, whose radio morphologies are often unresolved (e.g. Smolčić et al. 2017).

In this paper we present results from the study of the radio properties of the dominant galaxies of the 27-group low-richness subset of the complete local-volume groups sample (CLoGS), including new giant metrewave radio telescope (GMRT) 235 and 610 MHz observations of 25 systems. The CLoGS sample and the X-ray properties of the high-richness groups are described in more detail in O'Sullivan et al. (2017, hereafter Paper I) while the radio properties of the BGEs in the high-richness subsample are described in Kolokythas et al. (2018, hereafter Paper II). This paper continues the work described in paper II, presenting the properties of the central radio sources in the low-richness subsample and discussing the whole CLoGS sample for the first time. We examine the connection between the group environment and the dominant radio galaxies, the contribution of star formation on the radio emission of point-like radio sources, and provide a qualitative comparison of the radio emission that BGEs exhibit in high- and low-richness group subsamples. The paper is organized as follows: In Section 2 we briefly present the sample of galaxy groups, in Section 3 we describe the GMRT observations and the radio data analysis, in Section 4 we present the radio detection statistics of the BGEs, and in Section 5 their radio properties including information on the contribution of star formation on the radio emission. Section 6 contains the discussion of our results for the CLoGS sample as a whole, focusing on the detection statistics, the properties of the radio sources, their environment, and their energetics. The summary and the conclusions are given in Section 7. Radio images and information on the central galaxies of this sample work are presented in Appendices A to C. Throughout the paper we adopt the ΛCDM cosmology with $H_o = 70$ km s^{-1} Mpc^{-1}, $\Omega_m = 0.27$, and $\Omega_\Lambda = 0.73$. The radio spectral index α is defined as $S_\nu \propto \nu^{-\alpha}$, where S_ν is the flux density at the frequency ν. In general we quote 1σ uncertainties, and the uncertainties on our radio flux density measurements are described in Section 3.2.

2 THE COMPLETE LOCAL-VOLUME GROUPS SAMPLE

The CLoGS is an optically selected sample of 53 groups in the local universe ($D \leq 80$ Mpc), that is collected from the relatively not deep, all-sky Lyon Galaxy Group catalogue (LGG; Garcia 1993). Paper I provides a detailed description of the sample, its selection criteria, and the X-ray properties of the high-richness subsample, and we therefore only provide a brief summary of the selection here. The sample is statistically complete in the sense that, to the completeness limit of the LGG sample, it contains every group which meets our selection criteria. It is intended to be a representative survey of

groups in the local universe including studies of their radio, X-ray, and optical properties.

Constraints on the selection of CLoGS groups include: (i) a membership of at least four galaxies, (ii) the presence of $\geq$1 luminous early-type galaxy ($L_B > 3 \times 10^{10} L_\odot$) and (iii) a declination of $> -30^\circ$ in order to certify that the groups are observable from the GMRT and very large array (VLA). The group membership was extended and refined using the HyperLEDA catalogue (Paturel et al. 2003), based on which the group mean velocity dispersion and richness R parameter were estimated (R; number of member galaxies with log $L_B \geq 10.2$). Systems with $R > 10$ were not included in the sample as they were already known galaxy clusters, and systems with $R = 1$ were also excluded, as they were too poor to provide results on their physical parameters that would be reliable. From this process, we obtained a 53-group statistically complete sample that was divided into two subsamples: (i) the 26 high-richness groups with $R = 4-8$ (see Paper II) and (ii) the 27 low-richness groups with $R = 2$–3.

Distances to the CLoGS group-dominant galaxies are estimated from their recession velocities, corrected for Virgocentric flow. Inaccuracies in these distances will affect calculated values such as luminosities, but since we mainly consider relations between quantities presented on logarithmic scales, these differences will be small and will not significantly alter our findings (e.g. a distance error of 20 per cent would give a luminosity error of only 0.2 dex).

3 OBSERVATIONS AND DATA ANALYSIS

3.1 GMRT observations

Excluding six systems (NGC 315, NGC 524, NGC 1407, NGC 3325, NGC 3665, and NGC 4697; see Table 1) for which archival data were available, the low-richness sample of galaxy groups were observed using the GMRT in dual 235/610 MHz frequency mode during observing cycle 21, from 2011 November–2012 August. Each target was observed at both 235 and 610 MHz with the upper side band correlator (USB) for an average of ∼4 h on source. The total observing bandwidth at both frequencies is 32 MHz with the effective bandwidth at 235 MHz being ∼16 MHz.

At 610 MHz the data were obtained in 512 channels with a spectral resolution of 65.1 kHz for each channel, whereas at 235 MHz the data were obtained in 256 channels and a spectral resolution of 130.2 kHz for each channel. A detailed summary of the observations can be found in Table 1.

3.2 Data analysis

The data were processed using the SPAM pipeline[1] (Intema 2014). SPAM is a PYTHON based extension to the NRAO Astronomical Image Processing System (AIPS) package that includes direction-dependent calibration, radio frequency interference (RFI) mitigation schemes, along with imaging and ionospheric modelling, adjusting for the dispersive delay in the ionosphere. We provide here only a brief description of the SPAM pipeline to account for the data analysis procedure followed. For more details regarding the SPAM pipeline and the algorithms of the SPAM package see Intema et al. (2009, 2017).

The SPAM pipeline is run in two parts. In the first, pre-processing stage, the pipeline converts the raw LTA (Long Term Accumulation) format data collected from the observations into pre-calibrated visibility data sets for the total of the pointings observed (UVFITS format). The second stage converts these pre-calibrated visibility data of each pointing into a final Stokes I image (FITS format), via several repeated steps of (self)calibration, flagging, and wide-field imaging.

The final full-resolution images, corrected for the GMRT primary beam pattern, provide a field of view of $\sim 1.2^\circ \times 1.2^\circ$ at 610 MHz and $\sim 3^\circ \times 3^\circ$ at 235 MHz having a mean sensitivity for the data we observed (1σ noise level) of ∼0.09 mJy beam^{-1} at 610 MHz and ∼0.64 mJy beam^{-1} at 235 MHz (see Table 1). The measured sensitivities achieved from the analysis at both frequencies are in line with expectations from previous GMRT experience. The theoretical (thermal) noise values for our observations are 29 μJy beam^{-1} for 610 MHz and 80 μJy beam^{-1} for 235 MHz.[2] We note that the theoretical sensitivity is dependent on the square root of the time on source, and that there is therefore a variation in the sensitivity between different targets at the same frequency, as well as a difference in quality between the older archival hardware correlator data and the newer observations using the software correlator. The main source of the residual noise in our final images comes either from calibration uncertainties in the form of phase errors from rapidly varying ionospheric delays (especially at the lowest frequencies) or from dynamic range limitation due to limited data quality, calibration, and image reconstruction, that is mostly revealed by the presence of bright sources in the field. We also note that the full resolution of the GMRT is ∼6 arcsec at 610 MHz and ∼13 arcsec at 235 MHz with the $u - v$ range at 610 MHz being ∼0.1–50 kλ and at 235 MHz ∼0.05–21 kλ.

The flux density scale in the images was set from the available flux calibrators in each observing session (3C 48, 3C 286, and 3C 147) using the models from Scaife & Heald (2012). We adopt a flux density uncertainty of 5 per cent at 610 MHz and 8 per cent at 235 MHz, representing the residual amplitude calibration errors (Chandra, Ray & Bhatnagar 2004).

Out of the 27 BGEs in the CLoGS low-richness subsample, 25 were analysed in this study at both 610 and 235 MHz using the SPAM pipeline. The GMRT observations and images for NGC 315 at both 235 and 610 MHz are drawn from the earlier study of Giacintucci et al. (2011) and for NGC 1407 from the detailed follow-up work of Giacintucci et al. (2012), with the analysis of the observations being described in detail in those studies. In addition, we note that the GMRT data for NGC 5903 system were also analysed by the standard procedure followed as described in Kolokythas et al. (2015, 2018) and the results are found to be consistent with results from the SPAM pipeline output.

A total of 1400 MHz data were drawn primarily from the NRAO VLA Sky Survey (NVSS; Condon et al. 1998) and the study of Brown et al. (2011) that included measurements from the NVSS, Green Bank Telescope (GBT), and Parkes Radio Telescope, and from Condon et al. (2002) for NGC 252, NGC 1106, and NGC 5127.

[1]For more information on how to download and run SPAM see http://www.intema.nl/doku.php?id = huibintemaspam

[2]Calculated using the rms noise sensitivity equation in Section 2.1.6 from the GMRT Observer's Manual: http://gmrt.ncra.tifr.res.in/gmrt_hpage/Users/doc/manual/Manual_2013/manual_20Sep2013.pdf

Table 1. Details of the new GMRT observations analysed for this study, along with information on archival data analysed by the authors or by Giacintucci et al. (2011, marked *a*) and Giacintucci et al. (2012, marked *b*). For each source the first line displays the details for the 610 MHz and the second line for the 235 MHz. The columns give the LGG (Lyon Groups of Galaxies) number for each group, the BGE name, observation date, frequency, time on source, beam parameters, and the rms noise in the resulting images.

Group Name LGG	BGE	Observation Date	Frequency (MHz)	On source Time (min)	Beam, P.A. (Full array, arcsec × arcsec, °)	rms (mJy beam^{-1})
6	NGC 128	2011 Nov	610	157	5.32 × 4.06, −2.96	0.16
		2011 Nov	235	157	16.15 × 12.07, 74.34	1.90
12	NGC 252	2011 Nov	610	171	5.46 × 4.78, −44.72	0.06
		2011 Nov	235	171	16.16 × 14.17, 77.73	0.60
78	NGC 1106	2011 Nov	610	171	5.44 × 4.08, −2.47	0.10
		2011 Nov	235	171	14.83 × 10.31, −9.06	0.60
97	NGC 1395	2011 Nov	610	168	9.59 × 3.80, 37.03	0.10
		2011 Nov	235	168	28.74 × 9.20, 39.36	0.70
113	NGC 1550	2011 Dec	610	187	5.66 × 3.96, 88.52	0.04
		2011 Dec	235	187	14.28 × 10.65, 88.65	0.45
126	NGC 1779	2011 Dec	610	124	4.68 × 3.77, 34.90	0.05
		2011 Dec	235	124	12.67 × 9.68, 25.13	0.45
138	NGC 2292	2011 Dec	610	137	7.58 × 3.59, 36.19	0.05
		2011 Dec	235	137	20.11 × 9.22, 31.86	0.42
167	NGC 2768	2012 Jan	610	209	6.26 × 3.65, 49.03	0.03
		2012 Jan	235	209	16.31 × 9.49, 36.10	0.30
177	NGC 2911	2012 Jan	610	196	5.22 × 3.79, 60.15	0.10[1]
		2012 Jan	235	196	11.58 × 10.21, 39.92	0.30
232	NGC 3613	2012 Jan	610	212	5.79 × 3.63, 33.96	0.03
		2012 Jan	235	212	16.09 × 8.77, 22.22	0.26
255	NGC 3923	2012 Mar	610	156	7.33 × 4.02, −16.06	0.05
		2012 Mar	235	156	20.77 × 10.24, −10.22	0.45
329	NGC 4956	2012 Apr	610	199	5.24 × 3.96, 24.60	0.05
		2012 Apr	235	199	12.54 × 12.04, 11.54	0.48
341	NGC 5061	2012 May	610	200	6.54 × 3.68, 28.89	0.05
		2012 May	235	200	22.42 × 9.75, 38.61	0.50
350	NGC 5127	2012 Apr	610	200	6.56 × 4.42, −30.97	0.25
		2012 Apr	235	200	13.51 × 11.68, −27.35	0.65
360	NGC 5322	2012 May	610	199	5.07 × 4.00, −0.06	0.05
		2012 May	235	199	15.30 × 11.31, −49.08	0.70
370	NGC 5444	2012 May	610	160	4.42 × 3.99, 62.22	0.20
		2012 May	235	160	12.90 × 10.79, −61.85	0.80
376	NGC 5490	2012 May	610	160	4.14 × 3.55, 34.12	0.25
		2012 May	235	160	11.88 × 8.69, 35.44	1.85
383	NGC 5629	2012 May	610	227	4.95 × 3.96, 80.80	0.05
		2012 May	235	227	12.58 × 10.71, 83.01	0.40
398	NGC 5903	2012 May	610	181	5.78 × 3.81, 39.02	0.08
		2012 May	235	181	20.19 × 9.54, 45.97	0.60
457	NGC 7252	2012 Aug	610	199	5.18 × 4.36, 20.12	0.10
		2012 Aug	235	199	14.25 × 10.03, 19.52	0.60
463	NGC 7377	2012 Aug	610	217	5.41 × 3.92, 26.75	0.04
		2012 Aug	235	217	15.68 × 9.97, 17.05	0.40
Archival data						
14	NGC 315[a]	2008 Feb	610	380	5.20 × 5.00, 61.00	0.10
		2008 Aug	235	280	15.0 × 15.0, 0.00	0.70
23	NGC 524	2006 Mar	610	248	5.52 × 4.15, 89.20	0.18
		2006 Mar	235	248	11.79 × 9.89, 66.70	2.10
100	NGC 1407[b]	2009 Nov	610	270	8.20 × 4.40, 42.00	0.05
		2009 Nov	235	270	16.10 × 10.90, 36.00	0.25
205	NGC 3325	2004 May	610	63	10.52 × 3.78, 60.46	0.31
		2004 May	235	63	32.57 × 12.12, 57.37	38.0
236	NGC 3665	2009 Feb	610	248	5.08 × 4.10, 35.38	0.17
		2009 Feb	235	248	12.04 × 9.53, 32.99	0.78
314	NGC 4697	2006 Jan	610	347	5.44 × 4.46, −74.58	0.07
		2006 Jan	235	347	14.00 × 11.32, −64.90	1.14

Note: [1]The rms around the source area here is 0.2 mJy.

Table 2. Radio flux densities, radio power, and spectral indices of the sources in the low-richness subsample. The columns list the BGE name, redshift, flux density of each source at 235 and 610 MHz, the 235−610 MHz spectral index, the flux density at 1.4 GHz (drawn from the literature), the 235−1400 MHz spectral index, and the radio power at 235, 610, and 1400 MHz. All upper limits shown here from our analysis are 5× r.m.s. Five galaxies show no radio emission detected at 235, 610, or 1400 MHz. The references for the 1.4 GHz flux densities and the GMRT measurements from previous works are listed at the bottom of the table.

Source	Redshift (z)	$S_{235\,\mathrm{MHz}}$ ±8% (mJy)	$S_{610\,\mathrm{MHz}}$ ±5% (mJy)	$\alpha^{610\,\mathrm{MHz}}_{235\,\mathrm{MHz}}$ (±0.04)	$S_{1.4\,\mathrm{GHz}}$ (mJy)	$\alpha^{1400\,\mathrm{MHz}}_{235\,\mathrm{MHz}}$	$P_{235\,\mathrm{MHz}}$ (10^{23} W Hz^{-1})	$P_{610\,\mathrm{MHz}}$ (10^{23} W Hz^{-1})	$P_{1.4\,\mathrm{GHz}}$ (10^{23} W Hz^{-1})
NGC 128	0.0141	≤9.5	≤0.8	–	1.5 ± 0.5[a]	–	≤0.041	≤0.003	0.006
NGC 252	0.0165	≤3.0	0.9	–	2.5[b]	–	≤0.019	0.006	0.016
NGC 1106	0.0145	435.0	221.0	0.71	132 ± 4[b]	0.67 ± 0.04	2.122	1.078	0.645
NGC 1395	0.0057	≤3.5	3.6	–	1.1 ± 0.5[a]	–	≤0.002	0.002	0.0006
NGC 1550	0.0124	223.0	62.0	1.34	17 ± 2[a]	1.44 ± 0.06	0.752	0.209	0.057
NGC 1779	0.0111	4.6	2.6	0.60	5.4 ± 0.6[c]	−0.09 ± 0.05	0.011	0.006	0.013
NGC 2292	0.0068	≤2.1	≤0.3	–	–	–	≤0.002	≤0.0003	–
NGC 2768	0.0045	13.1	11.5	0.14	14 ± 1[a]	−0.04 ± 0.07	0.008	0.007	0.009
NGC 2911	0.0106	69.0	58.0	0.18	56 ± 2[a]	0.12 ± 0.04	0.166	0.139	0.135
NGC 3613	0.0068	≤1.3	≤0.2	–	0.3 ± 0.3[a]	–	≤0.002	≤0.0002	0.0004
NGC 3923	0.0058	5.0	2.1	0.91	1 ± 0.5[a]	0.90 ± 0.22	0.002	0.001	0.0005
NGC 4956	0.0158	≤2.4	≤0.3	–	–	–	≤0.014	≤0.002	–
NGC 5061	0.0069	≤2.5	0.8	–	–	–	≤0.002	0.001	–
NGC 5127	0.0162	5690	1630	1.32	1980[b]	0.59 ± 0.04	35.464	10.159	12.278
NGC 5322	0.0059	134.6	106.0	0.25	79.3 ± 2.8[c]	0.30 ± 0.04	0.135	0.106	0.080
NGC 5444	0.0131	≤12[d]	≤1[d]	–	–*	–	≤0.051	≤0.004	–
NGC 5490	0.0162	1140	815	0.36	1300 ± 100[a]	−0.07 ± 0.05	6.804	4.864	7.839
NGC 5629	0.0150	≤2.0	≤0.3	–	–	–	≤0.011	≤0.002	–
NGC 5903	0.0086	1830	970	0.68	321.5 ± 16.0[d]	0.99 ± 0.04	2.829	1.500	0.498
NGC 7252	0.0160	76.6	41.5	0.66	25.3 ± 1.2[c]	0.63 ± 0.04	0.397	0.215	0.132
NGC 7377	0.0111	2.7	2.1	0.27	3.4 ± 0.5[c]	−0.13 ± 0.07	0.007	0.005	0.009
Archival data/Previous work									
NGC 315[e]	0.0165	15411	≥2500	≤ 1.91	1800 ± 100[a]	1.20 ± 0.04	99.691	16.172	11.474
NGC 524	0.0080	≤10.5	2.0	–	3.1 ± 0.4[a]	–	≤0.015	0.003	0.004
NGC 1407[f]	0.0059	945	194	1.66	38 ± 2[f]	1.80 ± 0.04	0.603	0.124	0.024
NGC 3325	0.0189	≤191	≤1.55	–	–	–	≤1.449	≤0.012	–
NGC 3665	0.0069	225.2	149.0	0.43	113.2 ± 3.8[c]	0.39 ± 0.04	0.275	0.182	0.139
NGC 4697	0.0041	≤5.7	≤0.35	–	0.6 ± 0.5[a]	–	≤0.002	≤0.0001	0.0002

Notes: [a]Brown et al. (2011), [b]Condon et al. (2002), [c]Condon et al. (1998), [d]Upper limit was calculated from the maximum peak flux density on the position of the BGE as the phase calibration errors are too large due to a very bright 4C radio source nearby. The detection of the system in this case is limited by the dynamical range due to the very strong background source right next to the position of the BGE, [e]Giacintucci et al. (2011), [f]Giacintucci et al. (2012).
*Condon et al. (1998) (NVSS) and Brown et al. (2011) report for NGC 5444 a flux density at 1.4 GHz of ∼660 ± 20 which is a 4C nearby source.

4 RADIO DETECTIONS OF BRIGHTEST GROUP GALAXIES IN THE LOW-RICHNESS SAMPLE

The radio sources detected in the BGEs of each group were identified from the 235 and 610 MHz GMRT images and the available NVSS catalogue data. After that, we determined their morphology, calculated their flux densities (see Table 2), and their largest linear size (LLS). The GMRT images of the CLoGS low-richness groups at both frequencies along with more detailed information on these sources can be found in Appendixes A and B.

We find a radio detection rate of 82 per cent (22 of 27 BGEs) for the low-richness CLoGS sample, considering both GMRT frequencies and the 1.4 GHz surveys, with five galaxies being undetected at any of our three radio frequencies (NGC 2292, NGC 3325, NGC 4956, NGC 5444, and NGC 5629). Of these five undetected systems, NGC 5444 has previously been identified with a 4C source, but our higher resolution data shows that it is not related to the BGE (for more details see Section A20 and Fig. B20 for the radio image). NGC 3325 has a very high upper limit due to the high noise level from the analysis of the short archival observations available (see Table 2).

If we take into consideration the detection statistics only from the GMRT data, we find that 70 per cent of the BGEs are detected at 235 and/or 610 MHz (19 of 27 BGEs) with three BGEs (NGC 128, NGC 3613, and NGC 4697) being detected only at 1.4 GHz data. Fig. 1 presents the flux density distribution of all 53 CLoGS BGEs along with their upper limits (both high and low-richness subsamples) at 610 MHz with Fig. 2 presenting the distribution at 235 MHz. We observe that the majority of the BGEs have flux densities in the range 10–100 mJy, but that the 610 MHz flux density distribution of the low-richness subsample is shifted towards lower flux densities compared to the high-richness systems.

An upper limit of 5× the r.m.s. noise level in each image is used for the undetected radio sources, with the limits falling in the range ∼0.3−10 mJy for both subsamples and GMRT frequency ranges. However, while in Fig. 1 at 610 MHz we observe a similar number of radio non-detected BGEs (upper limits) between both subsamples, from Fig. 2 at 235 MHz the number of radio non-detected BGEs in the low-richness subsample is found to be almost twice than the number of non-detections in the high-richness subsample.

As in paper II, the limiting sensitivity of our sample is estimated based on the typical noise level of our images and the

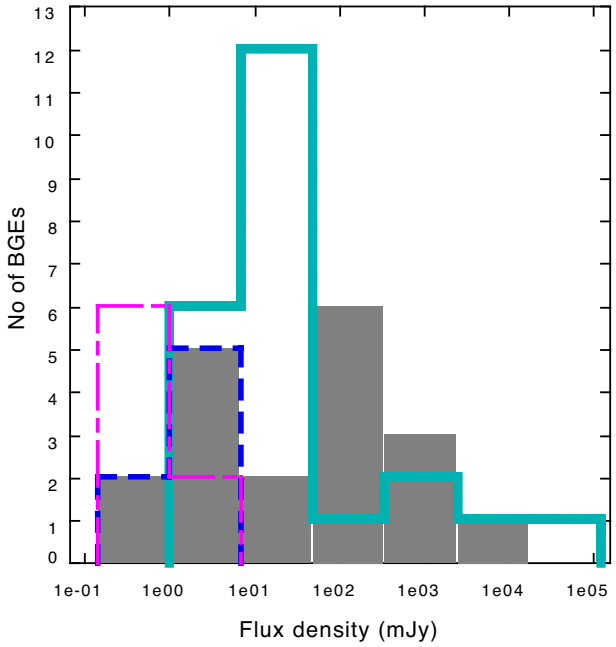

Figure 1. Flux density distribution of the CLoGS BGEs at 610 MHz, comparing the low-richness subsample (grey columns) with the high-richness systems (cyan solid line) from Paper II. The upper limits of the non-detected BGEs in the low-richness subsample are shown in magenta dot-dashed line whereas the equivalent upper limits in the high-richness subsample are shown in blue dashed line.

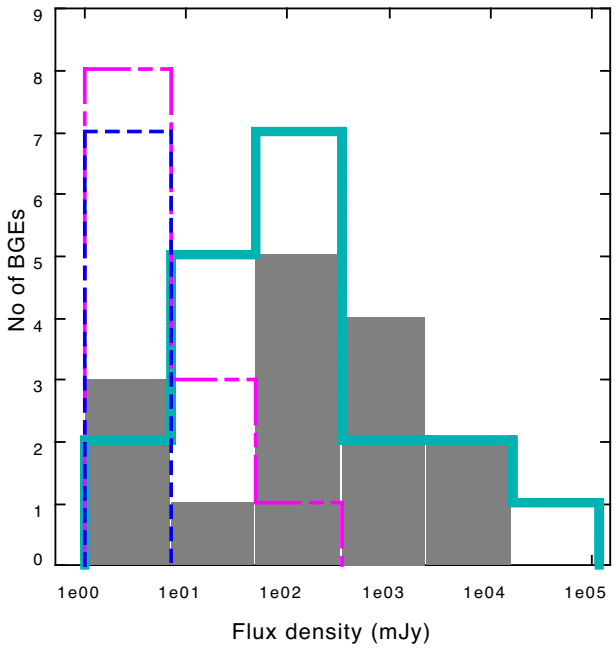

Figure 2. Same as in Fig. 1, but for the flux density distribution at 235 MHz.

maximum distance for the observed groups, which is 78 Mpc. The mean r.m.s from the analysis of the low-richness subsample (excluding the archival data) is ∼90 μJy beam^{-1} at 610 MHz and ∼640 μJy beam^{-1} at 235 MHz. This means that the limiting sensitivity in the low-richness subsample using the automated pipeline SPAM is $>3.3 \times 10^{20}$ W Hz^{-1} at 610 MHz or $>2.3 \times 10^{21}$ W Hz^{-1} at 235 MHz which is similar to the sensitivity power achieved for the high-richness subsample ($>2.9 \times 10^{20}$ W Hz^{-1} at 610 MHz or $>2.2 \times 10^{21}$ W Hz^{-1} at 235 MHz; Paper II). We note here that the limiting sensitivities are representing on average the total low-richness subsample and there may be individual radio sources detected at $>5\sigma$ level of significance at lower powers in nearby groups. The equivalent limit for NVSS 1400 MHz power sensitivity at CLoGS groups distance and level of significance for comparison is $>1.7 \times 10^{21}$ W Hz^{-1}.

5 RADIO PROPERTIES OF THE BRIGHTEST GROUP GALAXIES

We examine here the radio properties of the detected radio sources in the central galaxies of the low-richness sample. As in the high-richness sample, the sources present a range in size, power, and morphology. The GMRT images of the groups along with more details for these sources are presented in Appendices A and B.

5.1 Radio morphology

The radio structures found in the central galaxies have extents ranging from a few kpc (galactic scale) to hundreds of kpc (group scale). Table 3 lists the radio morphology for each source. We apply the radio morphology scheme described in Paper II, classifying our radio sources from our own GMRT 235 and 610 MHz analysis, the 1.4 GHz NVSS survey and from earlier studies on some of our BGEs. The purpose of this classification is to distinguish between the different classes of radio emission and provide information on their environment. Systems may belong to more than one category; when that is the case, the system is classified according to its most extended and prominent state/class.

The morphological classes are:

(i) point-like (unresolved) sources,
(ii) diffuse sources with no clear jet-lobe structure,
(iii) small-scale jets (<20 kpc),
(iv) large-scale jets (>20 kpc), and
(v) non-detections.

A subset of the large-scale jet sources have been shown by previous studies to be remnant systems, where the AGN is quiescent, but emission from the aging jets or lobes is still visible.

Table 3 summarizes the radio properties of the BGEs in the low-richness sample, showing their largest radio linear size, their radio morphology, their power at 235 MHz (see Section 5.3 below for more details) and an estimate of the energy injected into the IGM by the inflation of radio lobes by jet sources ($P_{\rm cav}$) calculated from the radio power at 235 MHz using the scaling relation from O'Sullivan et al. (2011; see also section 6.4):

$$\log P_{\rm cav} = 0.71\,(\pm0.11)\,\log P_{235} + 1.26\,(\pm0.12), \quad (1)$$

where $P_{\rm cav}$ and P_{235} are in units of 10^{42} erg s^{-1} and 10^{24} W Hz^{-1}.

We find that in the low-richness sample 14 central galaxies exhibit point-like radio emission, two host small-scale jets, five host large-scale jets (of which 1, NGC 1407, is a remnant jet; see below for details) with five BGEs being undetected at the frequencies we investigated, and only one system presenting a diffuse radio structure.

NGC 3665 and NGC 5322 are the two systems that exhibit a small-scale jet morphology and both present symmetrical structures and thin, straight jets (see Fig. B13 and B19) with similar sizes (see Table 3). The four currently active large-scale jet systems are all

Table 3. Morphological properties of CLoGS low-richness groups and their central radio sources. For each group we note the LGG number, the BGE name, the angular scale, the largest linear size (LLS) of the radio source, measured from the 235 MHz radio images unless stated otherwise, the radio morphology class, and lastly the energy output of any radio jets, estimated from the 235 MHz power using equation (1). The errors on the energy output were calculated based on the errors from scaling relation 1.

Group	BGE	Scale (kpc arcsec^{-1})	LLS (kpc)	Radio morphology	Energy output (radio) (10^{42} erg s^{-1})
LGG 6	NGC 128	0.291	$\leq 3^a$	Point	–
LGG 12	NGC 252	0.349	≤ 3	Point	–
LGG 14	NGC 315	0.354	1200^b	Large-scale jet	$93.13^{+64.97}_{-38.27}$
LGG 23	NGC 524	0.165	$\leq 2^c$	Point	–
LGG 78	NGC 1106	0.310	≤ 14	Point	–
LGG 97	NGC 1395	0.102	≤ 3	Point	–
LGG 100	NGC 1407	0.112	80^b	Remnant	–
LGG 113	NGC 1550	0.257	33	Large-scale jet	$2.89^{+0.02}_{-0.03}$
LGG 126	NGC 1779	0.218	≤ 4	Point	–
LGG 138	NGC 2292	0.145	–	–	–
LGG 167	NGC 2768	0.112	≤ 3	Point	–
LGG 177	NGC 2911	0.218	≤ 7	Point	–
LGG 205	NGC 3325	0.388	–	–	–
LGG 232	NGC 3613	0.156	$\leq 3^a$	Point	–
LGG 236	NGC 3665	0.156	16	Small-scale jet	$1.42^{+0.16}_{-0.18}$
LGG 255	NGC 3923	0.097	≤ 3	Point	–
LGG 314	NGC 4697	0.087	$\leq 3^a$	Point	–
LGG 329	NGC 4956	0.344	–	–	–
LGG 341	NGC 5061	0.136	≤ 2	Point	–
LGG 350	NGC 5127	0.349	244	Large-scale jet	$44.74^{+23.06}_{-15.22}$
LGG 360	NGC 5322	0.141	15^c	Small-scale jet	$0.86^{+0.15}_{-0.19}$
LGG 370	NGC 5444	0.291	–	–	–
LGG 376	NGC 5490	0.344	120 (30 at 610 MHz)	Large-scale jet	$13.84^{+3.65}_{-2.89}$
LGG 383	NGC 5629	0.325	–	–	–
LGG 398	NGC 5903	0.175	65^d	Diffuse	–
LGG 457	NGC 7252	0.320	≤ 14	Point	–
LGG 463	NGC 7377	0.223	≤ 5	Point	–

Note: [a]Measured from the 1.4 GHz image, [b] Giacintucci et al. (2011), [c] Measured from the 610 MHz image, [d] O'Sullivan et al. (2018a).

Fanaroff-Riley type I (FR I; Fanaroff & Riley 1974) radio galaxies with their jet/lobe components extending from several tens of kpc (e.g. 33 kpc; NGC 1550) to several hundreds of kpc (1200 kpc; NGC 315) away from their host galaxy.

Looking at the large-scale jet systems in more detail, NGC 1550 presents an unusually asymmetric FR I radio morphology with the eastern lobe roughly half as far from the optical centre of the galaxy as its western counterpart (see Fig. B6). Our GMRT data provides a considerably clearer view of the radio morphology than previous studies (e.g. Dunn et al.), revealing the previously unresolved lobes and a sharp z-bend in the western jet that produces an offset between the east and west jet axes. We will discuss this system in greater detail in a forthcoming paper (Kolokythas et al. in preparation).

In NGC 5490 we also observe an asymmetric morphology with the eastern jet detected to ∼50 kpc while the opposite side of the source breaks up into detached clumps of radio emission (see Fig. B21). NGC 5127 on the other hand, presents a normal symmetric double jet morphology (see Fig. B18) with NGC 315 hosting the giant FR I radio galaxy B2 0055 + 30 which has been extensively investigated at multiple frequencies and angular resolutions (e.g. Bridle et al. 1976, 1979; Venturi et al. 1993; Mack et al. 1997; Worrall et al. 2007; Giacintucci et al. 2011). NGC 315 presents two asymmetric jets, with one (northwest) being brighter and appearing bent backwards and the opposite (southeast) jet appearing much fainter and intermittent with the radio source having a total linear size of ∼1200 kpc (see Giacintucci et al. 2011).

NGC 1407 is the only radio galaxy in the low-richness sample classed as remnant radio source, as the radio spectral age analysis in the study of Giacintucci et al. (2012) revealed that a faint ∼300 Myr old, ultrasteep spectrum ($\alpha = 1.8$) radio plasma of ∼80 kpc surrounds the central jet source, which is a typical product of former AGN activity and characteristic of a dying radio galaxy.

The only diffuse radio source in the low-richness sample, appears in the galaxy group NGC 5903 (see Fig. B23). It has also been examined by several earlier studies at many different frequencies (e.g. Gopal-Krishna 1978; Gopal-Krishna et al. 2012; O'Sullivan et al. 2018a). It hosts a ∼75 kpc wide diffuse, steep-spectrum ($\alpha_{150}^{612} \sim 1.03$; O'Sullivan et al. 2018a) radio source whose origin may be through a combination of AGN activity and violent galaxy interactions (see A23). We note that NGC 5903 could also be categorized as a remnant system, but due to its complex origin and current state we consider it more conservative to class this system as diffuse.

5.2 Radio spectral index

Where possible, we estimate the spectral indices of each radio source in the frequency ranges 235−610 MHz and 235−1400 MHz. The radio spectral index of a source will, over time, steepen owing to synchrotron and inverse Compton losses, provided that there is no new source of electrons and no additional energy injection. Spectral index is therefore, in the absence of complicating factors, an indicator of source age.

Examining the radio sources in the low-richness sample, we find that only just over half the BGEs (15/27 galaxies; 56 per cent) are detected at both GMRT frequencies at 235 and 610 MHz. At this frequency range we find that four sources present steep radio spectra of $\alpha_{235}^{610} > 1$ (NGC 1550, NGC 5127, NGC 315, and NGC 1407) with NGC 315 and NGC 1407 presenting ultrasteep spectra of $\alpha_{235}^{610} \geq 1.91$ and $\alpha_{235}^{610} = 1.66$, respectively (see Table 2). However, in the study of Giacintucci et al. (2011) the flux density of NGC 315 at 610 MHz is quoted as underestimated, therefore the spectral index calculated must be considered an upper limit. For the same galaxy, Mack et al. (1997), using the WSRT at the same frequency (609 MHz) reported a flux density of 5.3 Jy, thus reducing the spectral index value of the radio source in NGC 315 to $\alpha_{235}^{609} = 1.11$. For NGC 1407, Giacintucci et al. (2012) reported that the radio spectral index value at the 235−610 MHz range was calculated after subtracting contributions in the flux densities at both frequencies from an inner double (young jets associated with the NGC 1407 AGN) and two point radio sources whose positions fall within the large-scale diffuse emission of the old radio lobes.

The rest of the 11 radio sources present α_{235}^{610} that ranges from very flat values of ∼0.1 to typical radio synchrotron spectra of ∼0.9. We find that the total mean spectral index value at the GMRT frequency range, leaving the two overestimated steep spectrum outliers out (NGC 315 and NGC 1407), is $\alpha_{235}^{610} = 0.60 \pm 0.16$ (for 13/15 radio sources).

Examining the radio spectral index distribution between 235 and 1400 MHz we find that four radio sources (NGC 1779, NGC 2768, NGC 5490, and NGC 7377), three of which exhibit a relatively flat spectral index in the 235−610 MHz range (all except NGC 1779 which has $\alpha_{235}^{610} = 0.60$), have flux densities greater at 1400 MHz than at 235 MHz, giving an inverted spectral index in the 235−1400 MHz range (see Table 2). Three of these four systems present weak point-like radio sources at both frequencies (NGC 1779, NGC 2768, and NGC 7377), hence the deviation from a power law of the observed flux density can be attributed to self-absorption of the lower frequency emission at 235 MHz as a result of the 'cosmic conspiracy' (see Cotton et al. 1980).

For the FR I radio jet system in NGC 5490, the observed inverted spectral index in the 235−1400 MHz range ($\alpha_{235}^{1400} = -0.07$) arises primarily from the difference in detected morphology between the two frequencies. The bright source close to NGC 5490 limits the sensitivity we were able to achieve at 235 MHz and probably prevented us from detecting all the corresponding radio emission from the source that has been picked up at 1400 MHz. The mean value of α_{235}^{1400} that we calculate for the 15/27 BGEs in the low-richness sample is 0.57 ± 0.16.

In Table 4 we list the mean values of the radio spectral indices for the point-like, small-scale, and large-scale jet radio morphologies in the low-richness sample. We neglected to include values for remnant jets and diffuse sources since these classes consist of only one system each. We find that large-scale jet systems present the steepest mean indices ($\alpha_{235}^{610} = 1.23 \pm 0.08$ and $\alpha_{235}^{1400} = 0.79 \pm 0.08$) in the low-richness sample, with small-scale jet systems exhibiting the flattest spectra, having similar values at both frequency ranges that we examined. The point-like radio sources are found to exhibit typical radio spectrum indices with the mean values being comparable within the uncertainties at both frequency ranges. In large-scale jet systems, the steeper mean spectral index seen in the 235−610 MHz frequency range can be attributed to low number statistics and detection sensitivity between the two frequency ranges, as NGC 315 presents an upper limit for α_{235}^{610} due to the flux density underestimation at 610 MHz (Giacintucci et al. 2011) and NGC 5490 presents an inverted spectrum at 235−1400 MHz reducing the mean at this frequency range (see below for more on NGC 5490).

Table 4. Mean spectral indices α_{235}^{610} and α_{235}^{1400} for the different radio morphology classes in the low-richness sample. The last column shows the number of sources used in calculating the means.

Radio morphology	Mean α_{235}^{610}	Mean α_{235}^{1400}	No. of sources
Point-like	0.50 ± 0.11	0.29 ± 0.11	7
Small-scale jet	0.34 ± 0.06	0.35 ± 0.06	2
Large-scale jet	1.23 ± 0.08	0.79 ± 0.08	4

Table 5. Spectral indices in the 235−610 MHz range for the cores and extended emission of those radio sources in our sample whose morphology is resolved at both frequencies. Columns show the group LGG number, the BGE name, and the spectral index α_{235}^{610} of the core and the surrounding emission in each source.

Group	BGE	Core α_{235}^{610}	Surrounding α_{235}^{610}
LGG 113	NGC 1550	0.94 ± 0.04	1.36 ± 0.04
LGG 236	NGC 3665	0.39 ± 0.04	0.44 ± 0.04
LGG 350	NGC 5127	0.77 ± 0.04	1.33 ± 0.04
LGG 376	NGC 5490	0.55 ± 0.04	0.02 ± 0.04

For the systems analysed in this paper, where it was possible to separate their extended emission from the main core at both 235 and 610 MHz, we calculated the spectral indices for their core and the extended components separately. We created images with matched resolution, cell size, uv range, and image pixel size at these two frequencies. Table 5 lists the spectral index values for the four systems that meet these criteria. In NGC 3665 we find that the spectral index does not differ between the two components. For two systems (NGC 1550 and NGC 5127) the spectral index in their cores is flatter, indicating either aging along their jets, self-absorption, or the presence of free–free emission. For NGC 5490 we find that the core (which is clearly detected) presents a fairly typical spectral index value of 0.55 ± 0.04 but that the extended emission has a very flat value of 0.02 ± 0.04. The extended low-surface brightness emission presents different morphology between 235 and 610 MHz, so the flat spectral index we measure is likely biased, and probably does not reflect the true index of the extended component. A more accurate measurement would require higher signal-to-noise ratio data and low resolution images to trace the extended emission at both frequencies.

5.3 Radio power in CLoGS BGEs

As in paper II, we calculate the radio power P_ν, for the low-richness sample BGEs as:

$$P_\nu = 4\pi D^2 (1+z)^{(\alpha-1)} S_\nu, \quad (2)$$

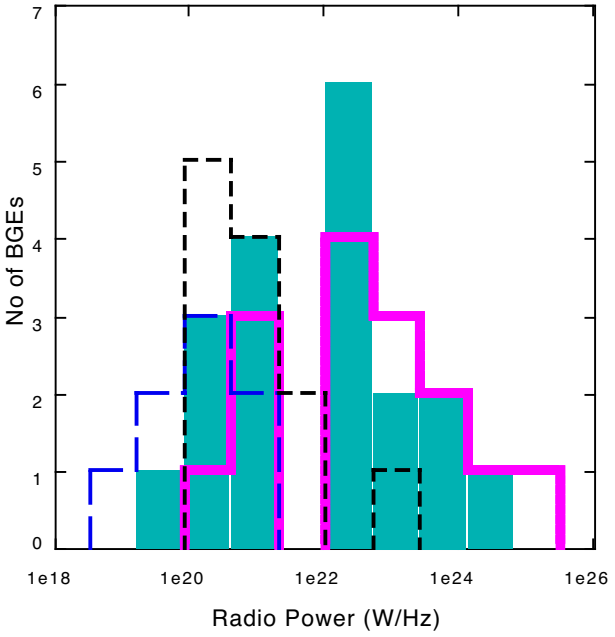

Figure 3. Radio power distribution of CLoGS BGEs in low-richness sample at 610 MHz (cyan columns) and 235 MHz (solid magenta line), with the upper limits at 610 MHz (blue dashed line) and at 235 MHz (black dotted line) also shown here.

where D is the distance to the source, α is the spectral index in the 235−610 MHz regime, z the redshift, and S_ν is the flux density of the source at frequency ν. For the systems that were detected at only one frequency the typical spectral index value of $\alpha = 0.8$ was used for the calculation (Condon 1992).

We find that in the low-richness sample the radio power of the detected radio sources in the BGEs is in the range 10^{19}–10^{25} W Hz^{-1}. Fig. 3 presents the radio power distribution of the BGEs from the low-richness subsample at both 235 and 610 MHz. The majority of the galaxies in Fig. 3 have low radio powers in the range between 10^{20} and 10^{21} and 10^{22}–10^{23} W Hz^{-1} with only one BGE exhibiting power in the range 10^{21}–10^{22} W Hz^{-1} (NGC 1779). The CLoGS low-richness sample contains two high-power sources with $P_{235\,\mathrm{MHz}} > 10^{24}$ W Hz^{-1}, both of which host large-scale bright radio jets (NGC 315 and NGC 5127). The radio power upper limits of the non-detected radio sources at 610 MHz extend to lower values (10^{19}–10^{20} W Hz^{-1}) than at 235 MHz, with the majority of the radio power upper limits at both frequencies seen between $\sim 5 \times 10^{19}$ and 5×10^{21} W Hz^{-1}. Only NGC 3325 presents an upper limit of an order of magnitude higher ($\sim 10^{23}$ W Hz^{-1}) compared to rest of the BGEs, due to the very high noise level in the image produced from the available archival data. We note that previously reported typical values of radio power at 235 and 610 MHz in BCGs range between $\sim 10^{23}$ and 5×10^{26} W Hz^{-1} (see e.g. Table 2; Yuan, Han & Wen 2016). The equivalent radio power statistics for the full sample will be discussed in Section 6.

5.3.1 *Radio-loudness in low-richness CLoGS sample BGEs*

Following Best et al. (2005), we consider as radio-loud systems with $P_{1.4\,\mathrm{GHz}} > 10^{23}$ W Hz^{-1}. In the low-richness sample we find that three BGEs have radio power higher than this value: NGC 315, NGC 5127, and NGC 5490 (see Table 6). While NGC 5903 and NGC 1106 have radio powers greater than 10^{23} W Hz^{-1} at 610 MHz

Table 6. Radio-loud AGN ($P_{1.4\,\mathrm{GHz}} > 10^{23}$ W Hz^{-1}) in the BGEs of the CLoGS low-richness sample. Columns show the LGG number, the BGE name, and the radio power at 1.4 GHz.

Group	BGE	$P_{1.4\,\mathrm{GHz}}$ (10^{23} W Hz^{-1})
LGG 14	NGC 315	11.5 ± 0.6
LGG 350	NGC 5127	12.3 ± 0.6
LGG 376	NGC 5490	7.8 ± 0.6

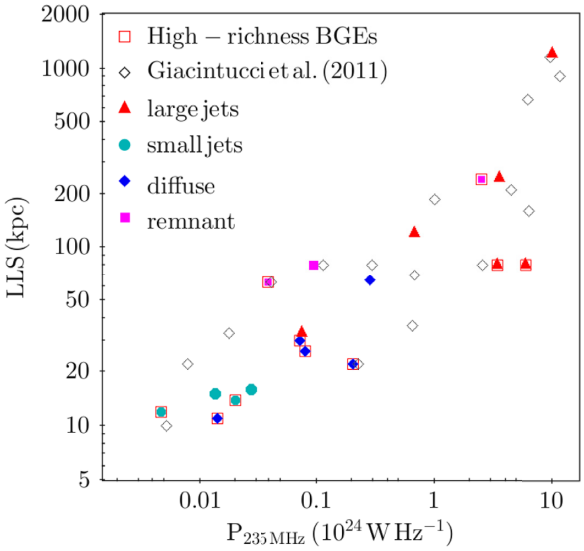

Figure 4. Radio power at 235 MHz plotted against the largest linear size for the full sample of CLoGS radio sources. Different symbols indicate the radio morphology of the radio sources. The points circumscribed by square box are representing BGEs from the high-richness sample, while those without the box are from the low-richness one. Open diamonds indicate systems in the Giacintucci et al. (2011) sample for comparison.

their corresponding flux density at 1.4 GHz is lower than the radio-loud limit, and we do not include them in the radio-loud category. In addition, the sensitivity limit of the NVSS survey and Brown et al. (2011) study guarantees that all the undetected systems at 1.4 GHz have radio powers below this limit. In Section 6 we discuss the equivalent statistics for the radio-loud systems in the full CLoGS sample.

5.3.2 *235 MHz radio power versus largest linear size*

It is well known that the linear size of FR I radio galaxies is proportional to their radio power (Ledlow, Owen & Eilek 2002). As in Paper II, we examine the relation between the 235 MHz power of our sources against their LLS. The relation was examined for the radio sources that were morphologically resolved, with their LLS being calculated across the longest extent of the detected radio emission, at the frequency at which the emission is most extended.

The resolved radio sources of the CLoGS low-richness central galaxies span a broad spatial scale from ∼15 kpc (small scale jets; NGC 5322) to >1200 kpc (large scale jets; NGC 315) with the corresponding 235 MHz radio powers being in the range of $\sim 10^{21}$ to $\sim 10^{25}$ W Hz^{-1}.

Fig. 4 shows the relation for the full CLoGS sample, along with the group systems from the study of Giacintucci et al. (2011). We

Table 7. Star formation rates calculated from FUV, and expected radio power at 610 MHz owing to star formation for the CLoGS low-richness sample point-like radio sources. For each system we list the SFR_{FUV}, the expected radio power at 610 MHz $P_{610\ expected}$ from the calculated SFR_{FUV}, the radio power at 610 MHz and 1.4 GHz ($P_{610\ MHz}$, $P_{1.4\,GHz}$), the molecular mass values (M_{H2}) drawn from O'Sullivan et al. (2018b), and the radio morphology of the source.

Group LGG	BGE	SFR_{FUV} (10^{-2} $M_\odot$ yr^{-1})	$P_{610\ expected}$ (10^{21} W Hz^{-1})	$P_{610\ MHz}$ (10^{21} W Hz^{-1})	$P_{1.4\,GHz}$ (10^{21} W Hz^{-1})	M_{H2} (10^8 $M_\odot$)	Morphology
6	NGC 128	4.9	0.13	1.25[a]	0.64	1.76 ± 1.5	Point
12	NGC 252	30.7	0.69	0.60	1.55	6.29 ± 0.79	Point
23	NGC 524	2.7	0.05	0.30	0.43	1.90 ± 0.23	Point
78	NGC 1106	26.7	0.94	107.80	64.50	6.81 ± 0.33	Point
97	NGC 1395	4.2	0.07	0.20	0.06	<0.27	Point
126	NGC 1779	–	–	–	1.31	4.57 ± 0.60	Point
167	NGC 2768	2.6	0.06	0.70	0.89	0.18 ± 0.01	Point
177	NGC 2911	3.2	0.11	13.90	13.53	2.66 ± 0.31	Point
232	NGC 3613	1.4	0.02	0.07[a]	0.04	<0.46	Point
255	NGC 3923	4.2	0.06	0.10	0.05	<0.29	Point
314	NGC 4697	3.1	0.04	0.05[a]	0.02	<0.07	Point
341	NGC 5061	2.7	0.04	0.08	0.04[b]	<0.43	Point
457	NGC 7252	36.8	1.29	21.50	13.16	58.00 ± 8.70	Point
463	NGC 7377	6.0	0.13	0.50	0.86	4.74 ± 0.44	Point

Notes: [a]The $P_{610\ MHz}$ was calculated by extrapolating the 610 MHz flux density from the available 1.4 GHz emission, using a spectral index of 0.8.
[b]The $P_{1.4\,GHz}$ was calculated by extrapolating the 1400 MHz flux density from the available 610 MHz emission, using a spectral index of 0.8.

find that our CLoGS radio sources are in agreement with the linear correlation between size and power found by Ledlow et al. (2002) and Giacintucci et al. (2011). In addition, our CLoGS BGEs range of luminosities and size distribution is in line with the measured values of radio sources from the recent LOFAR AGN study of Hardcastle et al. (2016) at 150 MHz over a greater redshift range (0−0.8) (see their fig. 18). We find that there is no significant difference in the spread of our group radio sources between the low and high-richness sample and confirm across group and cluster environments the linear correlation for the radio sources is valid and stands for almost four orders of magnitude at 235 MHz.

5.4 Star formation contribution in CLoGS radio sources

Although the source engine of radio jet systems is most certainly an AGN, it is not clear whether that is the case for the majority of the radio sources in the low-richness sample, which presents unresolved (point-like) radio morphology. Unless a luminous radio source is present ($P_{1.4\,GHz} > 10^{23}$ W Hz^{-1}), it is possible in these systems to confuse a compact central star forming region with AGN emission, as the beam sizes correspond to areas a few kiloparsecs across. Therefore, we examine the possibility of stellar contribution to the radio emission of the low-richness sample BGEs and in particular for those systems which exhibit low radio luminosities. We note here that in NGC 5903, the only system in the low-richness sample that presents a diffuse radio structure, the radio emission likely arises from a combination of AGN jet activity and galaxy interactions driven, and star formation cannot be a significant contributor to the radio luminosity of this system (see O'Sullivan et al. 2018a).

We estimate the expected contribution to the radio flux density from star formation using two methods. First, we use far-ultraviolet (FUV) fluxes from the Galaxy Evolution Survey GR6 catalogue[3] (Martin 2005) to estimate the star formation rate (SFR) from the calibration of Salim et al. (2007). We then calculate the expected 610 MHz radio emission from star formation at that rate using the relation of Garn et al. (2009) (more details on the star formation in CLoGS BGEs will be presented in a future paper; Kolokythas et al., in preparation).

Table 7 lists the calculated SFR from FUV and the estimated contribution to 610 MHz radio power, for the galaxies where star formation could potentially affect the radio flux density measurements in the low-richness sample (point-like systems). The only exception is NGC 1779, where no FUV flux was available. We consider that star formation dominates the radio emission if the expected radio power at 610 MHz of a BGE is >50 per cent of its actual $P_{610\,MHz}$ value. We find that in 6/13 systems, the luminosity from the detected radio emission exceeds by over an order of magnitude the expected radio luminosity from the FUV SFR, making these galaxies AGN dominated. In three galaxies (NGC 1395, NGC 3613, and NGC 7377), we find that star formation may contribute 20−40 per cent in the radio emission, in two galaxies may contribute significantly (50−60 per cent; NGC 3923 and NGC 5061), and in two systems (NGC 252 and NGC 4697) it appears to be the dominant source of radio emission with the expected radio luminosity from the FUV SFR exceeding or being similar to the observed radio luminosity. A plausible explanation as to why the expected radio luminosity from the FUV SFR exceeds the observed radio luminosity is that different phases of star formation can be traced by radio and FUV wavelengths – FUV from the largest young stars, radio from supernovae – therefore, a change in SFR over time could lead to a disagreement.

However, using as star formation estimate the FUV wavelength we probe star formation from only young massive stars and cannot account for internal extinction due to dust. In addition, the calibration from Salim et al. (2007) is only valid when the SFR remains constant over the lifetime of the UV-emitting stars ($<10^8$ yr). Thus the expected radio from SFR_{FUV} can hold for systems that do not present extreme recent starbursts or dust obscured star forming regions. NGC 7252 is likely an example of dust-obscured star formation in a post-starburst merger (see A24). We find SFR_{FUV} $\sim 0.04\,M_\odot\,yr^{-1}$, considerably less than the SFR estimated from the integrated far infrared (FIR) flux ($8.1\,M_\odot\,yr^{-1}$; O'Sullivan et al. 2015). However, as noted by George et al. (2018), radio and H α SFR estimates for NGC 7252 (Schweizer & Seitzer 2013) agree within a

[3]http://galex.stsci.edu/GR6/?page = mastform

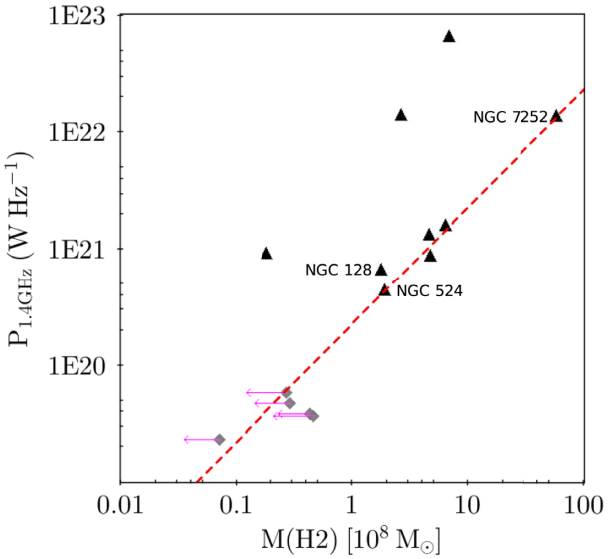

Figure 5. Radio power at 1.4 GHz in relation to molecular gas mass for the 14 point-like BGEs in the low-richness sample. The black triangles indicate systems with detected molecular gas and rhombus with arrows indicates systems with 3σ upper limits on molecular gas mass. The dashed red line represents the expected radio emission from star formation, assuming the molecular gas mass to star formation rate scaling relation of Gao & Solomon (2004).

factor of ∼2 with the FIR rate, and the implied degree of extinction is not unreasonable for such a gas-rich system. Modelling of the star formation history of the galaxy suggests peak SFRs of tens of $M_\odot$ yr^{-1} (Chien & Barnes 2010) within the last 200−600 Myr, and the discrepancy may also indicate a more recent decline in SFR, with the FUV tracing the youngest stars. While the high radio/FUV ratio might have been an indicator of a radio AGN, the low limit on the AGN X-ray luminosity (Nolan et al. 2004) and its radio morphology strongly suggest the radio emission from this system is dominated by star formation rather than an active nucleus (though there is evidence that the opposite was true in the past; Schweizer & Seitzer 2013).

In order to test whether the star formation contribution in the radio emission of point-like BGEs is consistent with typical SFRs in star forming galaxies, we also examine the expected radio power from star formation at 1.4 GHz, by converting molecular gas mass to SFR using the scaling relation of Gao & Solomon (2004). Following O'Sullivan et al. (2018b) in Fig. 5 we show the relation between the radio power at 1.4 GHz and the molecular gas mass ($M_{\rm H2}$) for the 14 point-like radio BGEs (see also Table 7). The dashed red line indicates the expected radio emission from star formation for the measured $M_{\rm H2}$. We find that along with NGC 7252, five more BGEs (NGC 128, NGC 252, NGC 524, NGC 1779, and NGC7377) fall close to the line for the expected radio emission from star formation along with the systems that present upper limits in molecular gas mass. The systems with upper limits (NGC 1395, NGC 3613, NGC 3923, NGC 4697, and NGC 5061) are seen about the line, indicating that they may be star formation dominated or have a significant contribution from star formation to their radio emission. In NGC 4697 the expected radio emission from $\rm SFR_{FUV}$ is >50 per cent hence we consider that this galaxy's radio emission is star formation dominated. The radio emission from three BGEs (NGC 1106, NGC 2768, and NGC 2911) is clearly far above the line, suggesting that their radio emission is AGN dominated.

While estimating the expected SFR from the molecular gas mass is not a direct measurement like that provided by the FUV flux, we find that both methods suggest that three systems are AGN dominated: NGC 1106, NGC 2768, and NGC 2911. We find inconsistent results between the two methods for NGC 524, NGC 7252, and NGC 128, which were classed as AGN dominated from their $\rm SFR_{FUV}$, but both methods produce similar results for the systems where star formation may make a significant contribution to the radio emission. We know that NGC 7252 is a starburst system and hence we consider its radio emission star formation dominated as well as in NGC 524 as is shown in Fig. 5. For NGC 128, where $P_{610\,\rm MHz}$ was estimated by the 1.4 GHz emission using a spectral index of 0.8, we consider that star formation may contribute significantly to the radio emission as is indicated by Fig. 5.

We therefore in summary, consider that in the low-richness sample, star formation most likely dominates the radio emission in 5/14 of the BGEs with point-like radio emission. It is possible that star formation may have a significant impact on our measurements of radio properties in six more (NGC 128 and the five BGEs with upper limits on molecular gas mass). We find that with certainty, the radio emission is AGN dominated in 3/14 point-like BGEs.

6 DISCUSSION

6.1 Detection statistics in CLoGS

Brightest group and cluster galaxies (BGGs and BCGs) in the local Universe are more likely to be detected in radio than the wider galaxy population. However, matching group and cluster samples to perform a comparison one has to be prudent, as very often different selection criteria have been applied (redshift, luminosity etc). The most recent statistical study by Hogan et al. (2015) using different X-ray selected cluster samples including systems out to redshift $z \sim 0.4$, reports a radio detection percentage for BCGs of 60.3 ± 7.7 per cent (from the ROSAT ESO Flux Limited X-ray/Sydney University Molonglo Sky Survey (REFLEX-SUMSS) sample (Böhringer et al. 2004), 62.6 ± 5.5 per cent (REFLEX-NVSS sample), and 61.1 ± 5.5 per cent from the extended Brightest Cluster Sample (eBCS; Ebeling et al. 2000). BCGs in the X-ray selected galaxy clusters of Ma, McNamara & Nulsen (2013) and Kale et al. (2015) (from the Extended Giant Metrewave Radio Telescope – GMRT – Radio Halo Survey; EGRHS; Venturi et al. 2007, 2008) present a radio detection rate of ∼52 and ∼48 per cent, respectively, from the NVSS (>3 mJy) and NVSS/FIRST catalogues.

In what may be the most relevant studies for CLoGS, Dunn et al. () used a sample of nearby early-type galaxies, most of which are in the centres of groups or clusters, and found a detection rate of ∼81 per cent (34/42) using NVSS and SUMSS data. Bharadwaj et al. (2014) report a ∼77 per cent (20/26) detection rate for the X-ray selected groups sample of Eckmiller, Hudson & Reiprich (2011) using the NVSS, SUMSS, and VLA Low frequency Sky Survey (VLSS, 74 MHz) radio catalogues.

In the CLoGS low-richness sample, considering only the 1.4 GHz data, we find a detection rate of ∼78 per cent (21/27 BGEs) with a similar detection rate of ∼81 per cent (21/26 BGEs) being found for the high-richness sample in Paper II. In total, the detection percentage at 1.4 GHz for the complete CLoGS sample is found to be ∼79 per cent (42/53 BGEs) which is in good agreement with the general trend of the high detection rate of brightest galaxies in the local Universe found by the studies mentioned above. We also note that CLoGS brightest group galaxies present a higher detection rate compared to those from clusters, as the average detection rate value

Table 8. Radio morphology occurrence for the BGEs in total CLOGS sample. The numbers for the high-richness sample are drawn from Paper II.

Radio morphology	Low-richness	High-richness	CLoGS total
Point-like	52% (14/27)	54% (14/26)	53% (28/53)
Non-detection	19% (5/27)	8% (2/26)	13% (7/53)
Large-scale jet	15% (4/27)	8% (2/26)	11% (6/53)
Diffuse emission	4% (1/27)	14% (4/26)	9% (5/53)
Small-scale jet	7% (2/27)	8% (2/26)	8% (4/53)
Remnant jet	4% (1/27)	8% (2/26)	6% (3/53)
Overall	82% (22/27)	92% (24/26)	87% (46/53)

for the BCGs from Hogan et al. (2015) is ∼61.3 ± 11 per cent. However, we note here that the latter study included cluster systems at a much greater volume ($z \sim 0.4$) than our CLoGS groups (∼20× farther) along with systems from the southern hemisphere, where the detection limit from SUMSS is ∼6 mJy (∼2.5× higher than NVSS). Hence, we treat this only as indicative of the relative detection statistics between groups and clusters.

The total radio detection rate for the CLoGS sample at any of the three radio frequencies (235, 610, and 1400 MHz) is ∼87 per cent (46/53 BGEs) which drops to ∼79 per cent (42/53 BGEs) if we consider only the GMRT data. In a comparison between the CLoGS two group subsamples, the radio detection rate was found to be slightly higher for the high-richness sample (24/26 BGEs, ∼92 per cent; Paper II) than for the low-richness groups (∼82 per cent 22/27 BGEs), but the difference is not statistically significant.

Examining the radio morphology appearance in CLoGS sample as a total, we find that more than half of the radio sources (∼53 per cent; 28/53) present point-like radio emission, followed by the BGEs with non-detections (∼13 per cent; 7/53). Large-scale jets are present in ∼11 per cent (6/53) of the BGEs, ∼9 per cent (5/53) host a diffuse radio source, ∼8 per cent (4/53) a small-scale jet, and ∼6 per cent (3/53) a remnant of an old radio outburst. In Table 8 we show the occurrence of radio morphology in total and in both subsamples. While both subsamples present a similar rate for small-scale and remnant jet morphologies, large-scale jet emission appears at higher rate in high-richness sample, with the most prominent difference between the two subsamples being the higher rate of undetected radio sources presented in the low-richness sample (∼19 per cent) compared to the high-richness one (∼8 per cent).

We find that, in total, 6/53 of our CLoGS BGEs can be considered as radio-loud following the definition by Best et al. (2005) ($P_{1.4\,\mathrm{GHz}} > 10^{23}\,\mathrm{W\,Hz^{-1}}$). This gives a percentage of ∼11 per cent radio-loud galaxies for CLoGS groups which is similar to the ∼13 per cent fraction of radio-loud galaxies found in low-mass clusters and groups ($10^{13} < M_{200} < 10^{14.2}$) by Lin & Mohr (2007).

We find that ∼9 ± 4 per cent (5/53) of the CLoGS BGEs are currently hosts of double-lobed radio galaxies (note that this excludes the lobeless double-jet system NGC 5490). This is slightly higher than the ∼8 ± 5 per cent (2/26; Paper I) found from the high-richness subsample but comparable within uncertainties. Huang & Chen (2010) find that the equivalent percentage of BCGs having double-lobed radio morphology, using a catalogue of ∼13 000 clusters from the maxBCG sample, is ∼4 per cent. It should also be noted that the remnant radio sources in our sample (NGC 1167, NGC 1407, and NGC 5044) all appear to be the remains of large-scale jet-lobe systems. Although this could suggest that double-lobed radio sources are more common in galaxy groups than clusters, this result needs to be treated with caution, since it is unclear how sensitive the cluster samples are to such steep spectrum remnant sources.

6.2 Spectral index of CLoGS BGEs

The spectral index of a radio source provides insight on the age and the nature of the mechanisms that give rise to radio emission (Lisenfeld & Völk 2000). In AGN, the most important mechanisms at high frequencies are inverse Compton losses and synchrotron emission which is produced by relativistic electrons spiralling down magnetic field lines. The cores of AGN usually present a flat radio spectrum as a result of self-absorption at low frequencies rather than a flat electron energy distribution, with a steep spectrum being observed from the extended emission (lobes) of an AGN.

For extended radio galaxies that lie in the centre of cool-core clusters and groups, the spectral index distribution is generally found to be 1−2 in the 235−610 MHz frequency range (Giacintucci et al. 2011). The spectral indices of these sources are thought to be steep owing to the confinement of the relativistic radio plasma by the surrounding intracluster medium (e.g. Fanti et al. 1995; Murgia et al. 1999). Bornancini et al. (2010), using a sample of maxBCG clusters and radio data from the Faint Images of the Radio Sky at Twenty-cm survey (FIRST; 1400 MHz), the NVSS (1400 MHz), the Westerbork Northern Sky Survey (WENSS; 325 MHz), and the Green Bank 6 cm Survey (GB6; 4850 MHz), calculated the mean value of the spectral index for BCGs between 325 MHz and 1.4 GHz to be $\alpha_{325}^{1400} = 0.65$. However, the authors did not select by radio morphology, and the inclusion in the spectral index calculation of radio point sources as well as jet-lobe systems probably explains the flatter mean index, showing that different morphological types of radio sources have an impact on the mean value of the spectral index.

In the CLoGS sample we are able to measure the 235–610 MHz spectral index in 34/53 BGEs. The mean spectral index for these radio sources is $\alpha_{235}^{610} = 0.68 \pm 0.23$, with a standard deviation of 0.55, whereas in the 235−1400 MHz frequency range, the mean radio spectral index for 33/53 BGEs is $\alpha_{235}^{1400} = 0.59 \pm 0.26$ with a standard deviation of 0.43. The uncertainties on the 1400 MHz flux for two galaxies, NGC 3923 and NGC 5982, were excluded from the error calculation of the mean α_{235}^{1400} as their high uncertainties provided for their low flux densities by Brown et al. (2011) are equivalent to their value (≤1 mJy see Table 2 and Paper II) which was increasing the average error on the mean by over a factor of 2.

The mean 235−610 MHz spectral index for CLoGS sample is significantly flatter than the value found by Giacintucci et al. (2011), probably owing to the inclusion of sources with a wide range of morphologies in our study. If we take into consideration the spectral indices only from the CLoGS large-scale and remnant jet systems in order to match with the extended group radio sources examined by the sample of Giacintucci et al. (2011), we find that $\alpha_{235}^{610} = 1.13 \pm 0.12$, in much better agreement. The mean α_{235}^{1400} of 0.59 ± 0.26 found for all our CLoGS systems is very close to the mean spectral index found by Bornancini et al. (2010) ($\alpha_{325}^{1400} = 0.65$) using a similar frequency range.

In the recent study of de Gasperin, Intema & Frail (2018), using data extracted from the NVSS (1400 MHz) and a reimaged version of the TGSS (TIFR GMRT Sky Survey, 147 MHz; Intema et al. 2017), the weighted average spectral index distribution α_{147}^{1400} for over a million extragalactic radio sources was found to be 0.79 with a standard deviation of 0.24 (for $S_\nu \propto \nu^{-\alpha}$). This is in agreement with previous results on extragalactic radio sources which found mean spectral indices α_{147}^{1400} in the range 0.75−0.8 (Ishwara-Chandra

Table 9. Mean spectral indices α_{235}^{610} and α_{235}^{1400} for the different radio morphology classes in the 53 group CLoGS sample.

Radio Morphology	Mean α_{235}^{610}	Mean α_{235}^{1400}
Point-like	0.47 ± 0.16	0.43 ± 0.26
Small-scale jet	0.52 ± 0.08	0.47 ± 0.08
Remnant jet	1.38 ± 0.07	1.11 ± 0.07
Large-scale jet	1.00 ± 0.10	0.72 ± 0.11
Diffuse emission	0.65 ± 0.09	0.72 ± 0.10

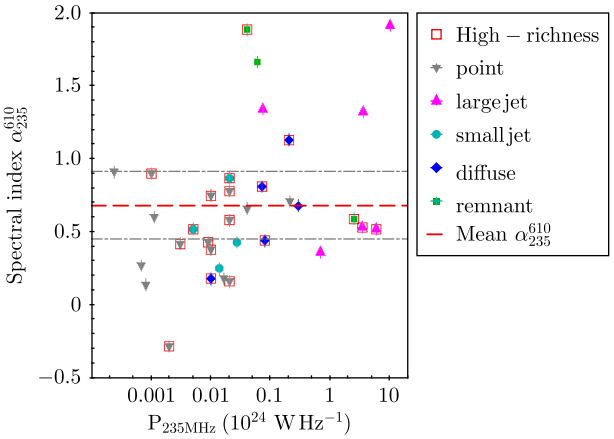

Figure 6. Spectral index α of CLoGS different radio morphologies in the frequency range 235−610 MHz, in relation to radio power at 235 MHz ($P_{235\,\mathrm{MHz}}$). The radio morphology of each source is indicated by the symbols, with the groups from the high-richness sample being marked by open squares.

et al. 2010; Intema et al. 2011). Although these studies include radio sources from various environments and redshifts, the CLoGS mean spectral index is consistent (within uncertainties) with their mean spectral indices.

Table 9 shows the mean spectral index values in the 235−610 and 235−1400 MHz bands for the different radio morphology classes in the full CLoGS sample. We find that point-like systems present a mean spectral index of $\alpha_{235}^{610} = 0.47 \pm 0.16$, diffuse radio sources a value of $\alpha_{235}^{610} = 0.65 \pm 0.09$ with jet systems (both small and large scale jets) presenting a steeper index of $\alpha_{235}^{610} = 0.81 \pm 0.13$. The mean 235–1400 MHz spectral index in jet systems is $\alpha_{235}^{1400} = 0.62 \pm 0.14$ with the mean value for point-like systems being $\alpha_{235}^{1400} = 0.43 \pm 0.26$.

As expected, jet systems show a somewhat steeper mean spectral index than point-like sources. In Fig. 6 we present the spectral index α_{235}^{610} distribution of CLoGS BGEs, in relation to their radio power at 235 MHz ($P_{235\,\mathrm{MHz}}$). We observe that point-like systems fall mainly about the calculated mean spectral index distribution. We also find that 50 per cent (3/6) of the large-scale jet systems exhibit steep α_{235}^{610} values with the other half having values close to the mean. While small-scale jet systems present small deviations in their spectral index values, we see that large-scale systems are divided between flat and very steep spectral α_{235}^{610} indices.

This divide in the large-scale jet sources might be explained by the different evolutionary stages of the jet systems (younger sources with flatter spectral indices, versus older or remnant sources with aged electron populations) or by the properties of the environment that the jets propagate into (e.g. bending lobes or confinement of electrons due to higher density environment). From Fig. 6 we also find a set of six radio sources that present a very steep spectrum, (>1), in the 235−610 MHz frequency range, with two of them being naturally remnant radio sources, which as expected present the largest deviation from the mean in our sample, another three sources being large-scale jet systems and the remaining one being of diffuse radio morphology.

Intema et al. (2011) categorized as ultrasteep spectrum (USS) those sources with spectral indices steeper than 1.3, and found that the fraction of USS found in the 153−1400 MHz frequency range is 3.8 per cent (16/417). This is in good agreement with earlier studies (e.g. 3.7 per cent; Sirothia et al. 2009). In the CLoGS sample, we find that only two radio sources present a spectral index steeper than 1.3 in the 235−1400 MHz frequency range (NGC 1407 and NGC 1550). This gives a USS fraction in good agreement with larger samples (3.8 per cent), but the result is strongly dependent on the detection limit at 235 MHz.

Table 10. Spiral fraction for the low-richness CLoGS groups. Spiral fraction (F_{sp}) is defined as the ratio of the number of late-type and unknown morphology galaxies to the total number of group members.

LGG	BGE F_{sp}	Spiral fraction
LGG 6	NGC 128	0.71
LGG 12	NGC 252	0.67
LGG 14	NGC 315	0.70
LGG 23	NGC 524	0.64
LGG 78	NGC 1106	0.87
LGG 97	NGC 1395	0.79
LGG 100	NGC 1407	0.50
LGG 113	NGC 1550	0.78
LGG 126	NGC 1779	0.92
LGG 138	NGC 2292	0.64
LGG 167	NGC 2768	0.89
LGG 177	NGC 2911	0.96
LGG 205	NGC 3325	0.96
LGG 232	NGC 3613	0.90
LGG 236	NGC 3665	0.86
LGG 255	NGC 3923	0.78
LGG 314	NGC 4697	0.87
LGG 329	NGC 4956	0.90
LGG 341	NGC 5061	0.86
LGG 350	NGC 5127	0.95
LGG 360	NGC 5322	0.84
LGG 370	NGC 5444	0.79
LGG 376	NGC 5490	0.50
LGG 383	NGC 5629	0.95
LGG 398	NGC 5903	0.78
LGG 457	NGC 7252	0.89
LGG 463	NGC 7377	0.60

6.3 Environmental properties

We investigate the relation between the radio morphology of a BGE and its near environment by examining the fraction of spiral galaxies in each group. The number of spiral galaxies that a group possesses is known to be connected to its dynamical age, as older systems will have had more opportunities for galaxy interaction and/or merging to drive morphological transformation.

We classify as spiral-rich (i.e. dynamically young) galaxy groups with a spiral fraction $F_{\mathrm{sp}} > 0.75$ (Bitsakis et al. 2010). In Table 10 we present the fraction of spiral galaxies in each group for the low-richness sample. The morphologies of the galaxies were drawn

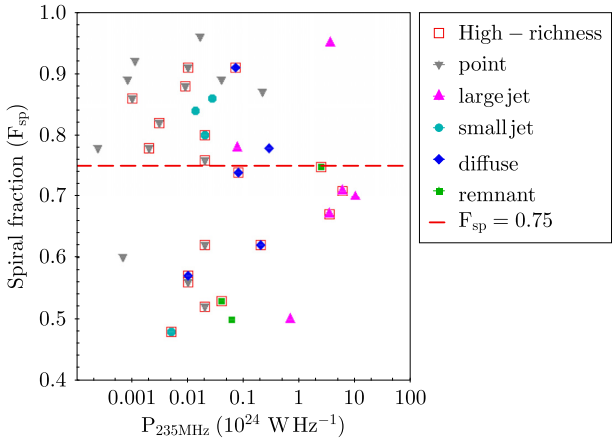

Figure 7. Spiral fraction F_{sp} plotted against 235 MHz radio power, with symbols indicating radio morphology of the BGE. Groups from the high-richness sample are marked with open squares.

from the HyperLEDA[4] catalogue, with morphological T-type < 0 galaxies being classified as early-type, and T-type ≥ 0 (or unknown) galaxies classed as late-type. As in Paper II, we define spiral fraction F_{sp} as the number of late-type galaxies over the total number of group members.

We find that 19/27 (70 ± 9 per cent) of the groups in the low-richness sample are spiral-rich and 8/27 (30 ± 9 per cent) are spiral-poor, whereas for the high-richness sample in Paper II we found that 11/26 (42 ± 10 per cent) of the groups are spiral-rich and 15/26 (58 ± 10 per cent) spiral-poor. Declining spiral fraction with richness may be an indication that galaxies undergo gradual morphological transformation if rich groups emerge over an extended period of time, or it may be a manifestation of galaxy downsizing, where galaxy-sized density peaks riding on larger-scale density fluctuations destined to form rich groups collapse early and rapidly to form preferentially spheroidal galaxies. Examining the CLoGS sample in total, 30/53 (57 per cent) of the groups are spiral-rich and 23/53 (43 per cent) are spiral-poor. Bitsakis et al. (2014), using a sample of 28 Hickson compact groups (HCGs; Hickson 1992), found that 46 per cent (13/28) were spiral-rich and 54 per cent (15/28) spiral-poor. Although Bitsakis et al. (2014) used a sample of compact groups that are likely to have higher galaxy interaction rates and thus evolve more rapidly than our systems, the spiral-rich fraction found in Bitsakis et al. (2014) is similar to our high-richness sample. This again demonstrates that richer groups are a conducive environment for galaxy evolution.

In Fig. 7 we show the relation between F_{sp} and the radio power at 235 MHz ($P_{235\,MHz}$) for all CLoGS systems whose BGEs are detected at 235 MHz. For the low-richness sample we find that all but one of the point-like systems appear in galaxy groups with higher spiral fractions (6/7; 86 per cent), with a mean spiral fraction of 0.84 ± 0.14. Jet systems in the low-richness subsample are also found to reside more often in a spiral-rich environment (4/6; 67 per cent) having a mean spiral fraction of 0.77 ± 0.17.

Looking at CLoGS groups as a whole, we find that the majority (75 per cent) of radio point-like systems detected at 235 MHz (12/16) reside in groups with high spiral fractions (dynamically young) with a mean spiral fraction of 0.78 ± 0.10. Jet systems, on the other hand, are found to be equally distributed between spiral-rich (5/10; 50 per cent) and spiral-poor environments (5/10; 50 per cent). However, we find the mean F_{SP} for jet sources (0.73 ± 0.14) is similar to that for point radio sources. Given the large uncertainties, this result cannot be regarded as statistically significant and larger sample of groups are required in order to confirm it. However, the even appearance of jet systems in both spiral-rich and spiral-poor groups suggests that the dynamical evolution of the galaxy population of a group has little influence on the radio jet activity of the BGE. This is of interest given the connection between jets and IGM properties found in paper I, where we found that more massive groups were more likely to have declining central temperature profiles and that the presence of jets was correlated with these cool cores and other evidence of rapid gas cooling. We might have expected that more dynamically evolved (i.e. spiral-poor) groups, which are likely to be more massive, would more commonly host central jet sources. Of the remnant jet sources, 2/3 (NGC 5044 and NGC 1407) reside in dynamically old groups (F_{SP} ∼0.5) while the third, NGC 1167, is the BGE of an X-ray faint group with a high spiral fraction (0.75). Diffuse radio sources, similar to jet systems, occur in groups with a wide range of spiral fractions (0.57–0.91) with 3/5 residing in high spiral fraction groups. Our X-ray analysis of the low-richness sample is not yet complete, and will be reported in a later paper, but our preliminary analysis suggests that 10/13 jet systems in the full CLoGS sample are hosted by X-ray bright groups with group-scale X-ray haloes. As reported in paper I, NGC 1167 is the BGE of an X-ray faint group with little or no hot gas, and in the low-richness sample we find two jet sources in systems with only galaxy-scale gas haloes. This suggests that even in low mass, less evolved groups, a hot gas-rich environment is preferable for jets (e.g. McNamara & Nulsen 2007). We examine the properties of jet-hosting BGEs in more detail in the next the section (Section 6.4).

6.4 Power output and properties of jet activity in CLoGS

As in Paper II, the energy output of jet sources in the low-richness sample is estimated using the P_{cav}–P_{235} scaling relation by O'Sullivan et al. (2011). This relation estimates the cavity power of a jet system based on the BGE's radio power at 235 MHz allowing the use of radio data as a proxy to estimate the AGN mechanical power output of radio jet systems. It has the benefit of providing with an estimate of the mechanical power output in the absence of direct calculations of cavity power (P_{cav}) from the X-rays. Table 3 shows the results from the calculations of the radio energy output. We find that the energy output values for the jet systems in the low-richness sample range from ∼10^{42} to 10^{44} erg s^{-1}, which is common for galaxy groups, but roughly an order of magnitude greater than the range found for the high-richness sample. The giant radio galaxy NGC 315 produces the difference in the upper bound of the range, and given the limited scale of our sample, the low- and high-richness subsamples are likely comparable.

For the BGEs in the CLoGS sample that present either an ongoing jet radio emission (large and small-scale jets; 10/53) or a past one (remnant jets; 3/53) we examine whether a correlation exists between the mass of the central black hole (BH) and their radio activity at 235 MHz. We calculate the BH masses for all CLoGS systems using the correlation of Ferrarese & Merritt (2000), estimating the mass of the BH from the central velocity dispersion of the host galaxy. This correlation is expressed as:

$$\log_{10}\left(\frac{M_{BH}}{M_{\odot}}\right) = \alpha + b\log_{10}\left(\frac{\sigma_o}{200\ \mathrm{km\ s^{-1}}}\right), \quad (3)$$

[4] http://leda.univ-lyon1.fr/

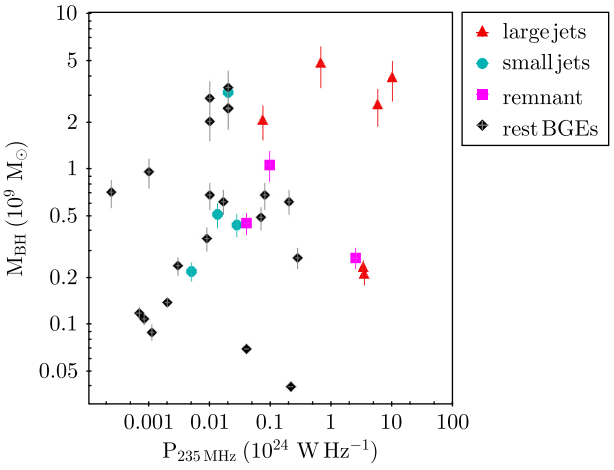

Figure 8. Black hole mass (M_{BH}) of different radio morphologies, in relation to radio power at 235 MHz ($P_{235\,MHz}$). The radio morphology of each group can be seen in different symbols, with the host BGEs other than jet systems being marked as 'rest of BGEs' in triangles.

where M_{BH} is the mass of the black hole in solar masses ($M_\odot$) and σ_o is the central velocity dispersion. The central velocities dispersions for 23/53 of our BGEs were drawn from the recent kinematic study of Loubser et al. (2018) with the values for the remaining 30 obtained from the HyperLeda[5] catalogue. We estimated the BH masses for all CLoGS BGEs (see Table C1) using the values for the parameters $a = 8.39 \pm 0.06$ and $b = 5.20 \pm 0.36$ given by the fit of the velocity dispersion−black hole mass relation in McConnell & Ma (2013).

We find that the BGE systems with 235 MHz detections (34/53) have BH masses in the range of $\sim 10^8$–5×10^9 $M_\odot$, with the majority of the systems having masses $\leq 10^9$ $M_\odot$. Fig. 8 shows the relation between the radio power at 235 MHz ($P_{235\,MHz}$) and the BH mass for different radio morphologies. Jet systems present in total a BH mass range of 0.2×10^9–5×10^9 $M_\odot$, with an average of $\sim 2.3 \pm 2.7 \times 10^9$ $M_\odot$ for the large-scale systems and $\sim 1.07 \pm 1.16 \times 10^9$ $M_\odot$ for the small scale.

We observe that 4/6 large-scale jet systems present a BH mass $> 2 \times 10^9$ $M_\odot$ with the hosts of 2/6 large-scale systems exhibiting a BH mass an order of magnitude less (NGC 193 and NGC 5127; $\sim 2 \times 10^8$ $M_\odot$). The most extended large-scale radio jet system in CLoGS ($\sim$1200 kpc; NGC 315) presents a BH mass estimate of $\sim 3.8 \times 10^9$ $M_\odot$. The recent study of Horellou et al. (2018) reports a BH mass of $\sim 1.6 \times 10^9$ $M_\odot$ for the BGE that hosts the giant radio source 'Double Irony' ($\sim$1100 kpc), which is equivalent to the BH mass that we find for NGC 315. We observe that 5/8 systems with BH mass $\geq 10^9$ $M_\odot$ are large-scale jet systems. For the systems that have no radio emission detected at any frequency (7/53) we find that their BH mass ranges $\sim 0.4 \times 10^8$–9×10^8 $M_\odot$ with an average of $2.8 \pm 2.5 \times 10^8$ $M_\odot$ which is on order of magnitude lower than the host BGEs of large-scale / jet systems.

On the other hand, the majority of small-scale jet systems (3/4) presents BH masses $\sim 2 - 5 \times 10^8$ $M_\odot$ with only one system, NGC 1060, which is known as a dynamically interacting group (O'Sullivan et al. 2017) having a BH mass of $\sim 3.1 \times 10^9$ $M_\odot$. We also note that only 10 BGEs present BH masses $> 10^9$ $M_\odot$ with all of them being known to be embedded in an extended X-ray environment (Paper II and Sun et al. 2003 for NGC 1550).

From Fig. 8 we observe a mild trend that suggests higher BH masses are linked with highest radio powers, as found by previous studies (e.g. Franceschini, Vercellone & Fabian 1998; Liu, Jiang & Gu 2006). However, we do not see a strong correlation between radio power at 235 MHz and the BH mass of the host BGEs in jet systems. There is a broad dispersion in radio power for a given BH mass for our CLoGS BGEs suggesting that a certain threshold value of BH mass may be necessary (but not on its own sufficient) to produce a powerful radio source, as suggested by a study of nearby field and group elliptical galaxies by Vaddi et al. (2016). This may indicate that jet activity depends more closely on environmental processes and the fuel that is available, rather than the mass of the host BGE's BH. In the diverse environment of galaxy groups we find that BH mass is not the main drive for the occurrence of jet emission, in agreement with the recent study of Sabater et al. (2019) in a sample of nearby AGN in the LOFAR Two-meter Sky Survey (LoTSS). Environmental mechanisms such as interactions, radiative cooling of the IGM, and precipitation of cold molecular gas are most likely prominent drivers for jet emission in galaxy groups. In addition to the effects of the large-scale environment, the efficiency of gas accretion and the BH spin likely also play a role in the large radio power dispersion seen for our group BGES at a given BH mass (e.g. Baum, Zirbel & O'Dea 1995).

7 CONCLUSIONS

In this paper we have presented the GMRT radio observations of the BGEs from the low-richness CLoGS sample at 235 and 610 MHz. Combining with the study of the high-richness sample from Paper II we present results and statistics from the complete CLoGS sample. The CLoGS low-richness sample is found to have a radio detection rate of 82 per cent (22 of 27 BGEs) at 235, 610, or 1400 MHz, with three radio sources being characterized as radio loud ($P_{1.4\,GHz} > 10^{23}$ W Hz^{-1} – NGC 315, NGC 5127, and NGC 5490). The overall detection rate of the CLoGS sample as a whole is 87 per cent (46 of 53 BGEs), a result which confirms the high radio detection rate of dominant galaxies in groups or clusters in the nearby Universe. We find that CLoGS group-dominant radio galaxies exhibit radio powers in the range of 10^{20}–10^{25} W Hz^{-1}.

Examining the radio morphology, we find that the majority of the groups in the CLoGS sample, $\sim$53 per cent (28/53) have a point-like radio morphology while $\sim$13 per cent (7/53) of groups are not detected in radio at any frequency. $\sim$25 per cent (13/53) of the groups are found to be hosting currently or recently active small/large scale jets and the remaining $\sim$9 per cent (5/53) host diffuse radio sources. The size of the extended CLoGS radio sources spans over three orders of magnitude from $\sim$10 to 1200 kpc.

For the very low-powered unresolved point-like radio sources in the CLoGS low-richness sample using the expected radio emission from SFR_{FUV} and the expected radio emission from the conversion of molecular gas to star formation, we find that 3/14 are AGN dominated (NGC 1106, NGC 2768, and NGC 2911), and 5/14 sources (NGC 128, NGC 1395, NGC 3613, NGC 3923, and NGC 5061) probably have a significant contribution (20–50 per cent) to their radio emission from star formation. In 6/14 point-like radio sources (NGC 252, NGC 524, NGC 1779, NGC 4697, NGC 7252, and NGC7377) we find that the stellar population likely dominates the radio emission.

[5] http://leda.univ-lyon1.fr/

In the CLoGS low-richness sample only 15/27 galaxies are detected at both 610 and 235 MHz with 2/15 sources exhibiting ultrasteep radio spectra with $\alpha_{235}^{610} > 1.3$ (NGC 315 and NGC 1407). The mean spectral index value for 13/15 sources is $\alpha_{235}^{610} = 0.60 \pm 0.16$ with the equivalent mean value in the 235−1400 MHz frequency range measured to be $\alpha_{235}^{1400} = 0.57 \pm 0.16$. In the full CLoGS sample we are able to measure a spectral index for 34/53 BGEs, and the mean spectral index is $\alpha_{235}^{610} = 0.68 \pm 0.23$. In the 235−1400 MHz frequency range the mean spectral index for 33/53 BGEs is measured to be $\alpha_{235}^{1400} = 0.59 \pm 0.26$. Jet systems are found to exhibit steeper mean α_{235}^{610} than point-like systems. Roughly 4 per cent of our sources have ultrasteep spectral indices ($\alpha_{235}^{610} > 1.3$), in good agreement with the earlier studies of Intema et al. (2011) and Sirothia et al. (2009).

Considering the group environments in which the BGEs are located, we find that 57 per cent (30/53) of the CLoGS groups are spiral-rich with 43 per cent (23/53) being spiral-poor. Comparing the mean spiral fraction (F_{sp}) to BGE radio morphology, we find that the majority (75 per cent) of radio point-like systems are found in dynamically young group systems (mean spiral fraction of 0.78 ± 0.10), with jet systems appearing equally in both dynamically young and old group systems, meaning that groups may form/host jets at any stage of their evolution. Our three remnant jet systems are also split between spiral-rich and spiral-poor groups, and BGEs which host diffuse, non-jet radio sources appear in groups with a wide range of spiral fractions.

We estimate the mechanical power output of the jet sources in the CLoGS low-richness sample from their 235 MHz luminosity, and find it to be in the range $\sim 10^{42}-10^{44}$ erg s^{-1}. This is typical for galaxy groups, but about an order of magnitude greater than the range of powers measured in our high-richness subsample. A combined X-ray and radio analysis will be needed to explore the reliability and origin of this difference.

Lastly, for all radio detected CLoGS groups, we find only a mild positive trend between the BH mass of the BGE and its radio power at 235 MHz. We do not find a correlation between the central BH mass and jet activity. Although a certain minimum black hole mass is necessary to form jets, we also suggest that it is not the most essential prerequisite for the formation of a jet, in agreement with other recent studies (e.g. Vaddi et al. 2016; Sabater et al. 2019).

ACKNOWLEDGEMENTS

The GMRT staff are gratefully acknowledged for their assistance during data acquisition for this project. GMRT is run by the National Centre for Radio Astrophysics of the Tata Institute of Fundamental Research. E. O'Sullivan acknowledges support for this work from the National Aeronautics and Space Administration through Chandra Awards GO6-17121X and GO6-17122X, issued by the Chandra X-ray Observatory Center, which is operated by the Smithsonian Astrophysical Observatory for and on behalf of NASA under contract NAS8-03060, and through the Astrophysical Data Analysis programme, award NNX13AE71G. S. Giacintucci acknowledges support for basic research in radio astronomy at the Naval Research Laboratory by 6.1 Base funding. Some of this research was supported by the EU/FP7 Marie Curie award of the IRSES grant CAFEGROUPS (247653). We acknowledge the use of the HyperLeda database (http://leda.univ-lyon1.fr). This research has made use of the NASA/IPAC Extragalactic Database (NED) which is operated by the Jet Propulsion Laboratory, California Institute of Technology, under contract with the National Aeronautics and Space Administration.

REFERENCES

Alexander D. M., Swinbank A. M., Smail I., McDermid R., Nesvadba N. P. H., 2010, MNRAS, 402, 2211
Alonso S., Mesa V., Padilla N., Lambas D. G., 2012, A&A, 539, A46
Bardelli S. et al., 2010, A&A, 511, A1
Baum S. A., Zirbel E. L., O'Dea C. P., 1995, ApJ, 451, 88
Bekki K., Shioya Y., Tanaka I., 1999, ApJ, 520, L99
Bernardi M., Hyde J. B., Sheth R. K., Miller C. J., Nichol R. C., 2007, AJ, 133, 1741
Best P. N., Kauffmann G., Heckman T. M., Brinchmann J., Charlot S., Ivezić Ž., White S. D. M., 2005, MNRAS, 362, 25
Bharadwaj V., Reiprich T. H., Schellenberger G., Eckmiller H. J., Mittal R., Israel H., 2014, A&A, 572, A46
Bîrzan L., McNamara B. R., Nulsen P. E. J., Carilli C. L., Wise M. W., 2008, ApJ, 686, 859
Bîrzan L., Rafferty D. A., Nulsen P. E. J., McNamara B. R., Röttgering H. J. A., Wise M. W., Mittal R., 2012, MNRAS, 427, 3468
Bitsakis T., Charmandaris V., Le Floc'h E., Díaz-Santos T., Slater S. K., Xilouris E., Haynes M. P., 2010, A&A, 517, A75
Bitsakis T., Charmandaris V., Appleton P. N., Díaz-Santos T., Le Floc'h E., da Cunha E., Alatalo K., Cluver M., 2014, A&A, 565, A25
Böhringer H. et al., 2004, A&A, 425, 367
Bornancini C. G., O'Mill A. L., Gurovich S., Lambas D. G., 2010, MNRAS, 406, 197
Bridle A. H., Davis M. M., Meloy D. A., Fomalont E. B., Strom R. G., Willis A. G., 1976, Nature, 262, 179
Bridle A. H., Davis M. M., Fomalont E. B., Willis A. G., Strom R. G., 1979, ApJ, 228, L9
Brown M. J. I., Jannuzi B. T., Floyd D. J. E., Mould J. R., 2011, ApJ, 731, L41
Chandra P., Ray A., Bhatnagar S., 2004, ApJ, 612, 974
Chien L.-H., Barnes J. E., 2010, MNRAS, 407, 43
Condon J. J., 1992, ARA&A, 30, 575
Condon J. J., Cotton W. D., Broderick J. J., 2002, AJ, 124, 675
Condon J. J., Cotton W. D., Greisen E. W., Yin Q. F., Perley R. A., Taylor G. B., Broderick J. J., 1998, AJ, 115, 1693
Cotton W. D. et al., 1980, ApJ, 238, L123
de Gasperin F., Intema H. T., Frail D. A., 2018, MNRAS, 474, 5008
De Lucia G., Blaizot J., 2007, MNRAS, 375, 2
Ebeling H., Edge A. C., Allen S. W., Crawford C. S., Fabian A. C., Huchra J. P., 2000, MNRAS, 318, 333
Eckmiller H. J., Hudson D. S., Reiprich T. H., 2011, A&A, 535, A105
Eke V. R., Baugh C. M., Cole S., Frenk C. S., King H. M., Peacock J. A., 2005, MNRAS, 362, 1233
Fanaroff B. L., Riley J. M., 1974, MNRAS, 167, 31P
Fanti C., Fanti R., Dallacasa D., Schilizzi R. T., Spencer R. E., Stanghellini C., 1995, A&A, 302, 317
Ferrarese L., Merritt D., 2000, ApJ, 539, L9
Forbes D. A. et al., 2006, Publ. Astron. Soc. Aust., 23, 38
Franceschini A., Vercellone S., Fabian A. C., 1998, MNRAS, 297, 817
Fukugita M., Hogan C. J., Peebles P. J. E., 1998, ApJ, 503, 518
Gao Y., Solomon P. M., 2004, ApJ, 606, 271
Garcia A. M., 1993, A&AS, 100, 47
Garn T., Green D. A., Riley J. M., Alexander P., 2009, MNRAS, 397, 1101
Geller M. J., Huchra J. P., 1983, ApJS, 52, 61
George K. et al., 2018, A&A, 614, A130
Giacintucci S. et al., 2011, ApJ, 732, 95
Giacintucci S. et al., 2012, ApJ, 755, 172
Gitti M., McNamara B. R., Nulsen P. E. J., Wise M. W., 2007, ApJ, 660, 1118
Gitti M., Brighenti F., McNamara B. R., 2012, Adv. Astron., 2012, 950641
Gopal-Krishna, 1978, MNRAS, 185, 579

Gopal-Krishna, Mhaskey M., Wiita P. J., Sirothia S. K., Kantharia N. G., Ishwara-Chandra C. H., 2012, MNRAS, 423, 1053
Gozaliasl G. et al., 2018, MNRAS, 475, 2787
Graham A., Lauer T. R., Colless M., Postman M., 1996, ApJ, 465, 534
Grossová R. et al., 2019, MNRAS, 488, 1917
Haines C. P. et al., 2018, MNRAS, 477, 4931
Hardcastle M. J. et al., 2016, MNRAS, 462, 1910
Hickson P., Mendes de Oliveira C., Huchra J. P., Palumbo G. G., 1992, ApJ, 399, 353
Hogan M. T. et al., 2015, MNRAS, 453, 1201
Horellou C. et al., 2018, A&A, 620, A19
Huang M.-L., Chen L.-. wen ., 2010, IAUS, 267, 110
Huchra J. P., Geller M. J., 1982, ApJ, 257, 423
Intema H. T., 2014, ASInC, 13, 469
Intema H. T., van der Tol S., Cotton W. D., Cohen A. S., van Bemmel I. M., Röttgering H. J. A., 2009, A&A, 501, 1185
Intema H. T., van Weeren R. J., Röttgering H. J. A., Lal D. V., 2011, A&A, 535, A38
Intema H. T., Jagannathan P., Mooley K. P., Frail D. A., 2017, A&A, 598, A78
Ishwara-Chandra C. H., Sirothia S. K., Wadadekar Y., Pal S., Windhorst R., 2010, MNRAS, 405, 436
Kale R., Venturi T., Cassano R., Giacintucci S., Bardelli S., Dallacasa D., Zucca E., 2015, A&A, 581, A23
Kolokythas K., O'Sullivan E., Giacintucci S., Raychaudhury S., Ishwara-Chandra C. H., Worrall D. M., Birkinshaw M., 2015, MNRAS, 450, 1732
Kolokythas K., O'Sullivan E., Raychaudhury S., Giacintucci S., Gitti M., Babul A., 2018, MNRAS, 481, 1550
Ledlow M. J., Owen F. N., Eilek J. A., 2002, New Astron. Rev., 46, 343
Liang L., Durier F., Babul A., Davé R., Oppenheimer B. D., Katz N., Fardal M., Quinn T., 2016, MNRAS, 456, 4266
Lilly S. J. et al., 2009, ApJS, 184, 218
Lin Y.-T., Mohr J. J., 2007, ApJS, 170, 71
Lisenfeld U., Völk H. J., 2000, A&A, 354, 423
Liu Y., Jiang D. R., Gu M. F., 2006, ApJ, 637, 669
Liu F. S., Mao S., Deng Z. G., Xia X. Y., Wen Z. L., 2009, MNRAS, 396, 2003
Loubser S. I., Hoekstra H., Babul A., O'Sullivan E., 2018, MNRAS, 477, 335
Mack K.-H., Klein U., O'Dea C. P., Willis A. G., 1997, A&AS, 123, 423
Magliocchetti M., Brüggen M., 2007, MNRAS, 379, 260
Ma C.-J., McNamara B. R., Nulsen P. E. J., 2013, ApJ, 763, 63
Malavasi N., Bardelli S., Ciliegi P., Ilbert O., Pozzetti L., Zucca E., 2015, A&A, 576A, 101
Martin C., GALEX Team, 2005, IAUS, 216, 221
McConnell N. J., Ma C.-P., 2013, ApJ, 764, 184
McNamara B. R., Nulsen P. E. J., 2007, ARA&A, 45, 117
McNamara B. R., Nulsen P. E. J., Wise M. W., Rafferty D. A., Carilli C., Sarazin C. L., Blanton E. L., 2005, Nature, 433, 45
Miles T. A., Raychaudhury S., Forbes D. A., Goudfrooij P., Ponman T. J., Kozhurina-Platais V., 2004, MNRAS, 355, 785
Morganti R., Fogasy J., Paragi Z., Oosterloo T., Orienti M., 2013, Science, 341, 1082
Moss C., Whittle M., 2000, MNRAS, 317, 667
Murgia M., Fanti C., Fanti R., Gregorini L., Klein U., Mack K.-H., Vigotti M., 1999, A&A, 345, 769
Nolan L. A., Ponman T. J., Read A. M., Schweizer F., 2004, MNRAS, 353, 221
O'Sullivan E., Giacintucci S., David L. P., Vrtilek J. M., Raychaudhury S., 2011, MNRAS, 411, 1833
O'Sullivan E., Combes F., Hamer S., Salomé P., Babul A., Raychaudhury S., 2015, A&A, 573, A111
O'Sullivan E. et al., 2017, MNRAS, 472, 1482
O'Sullivan E., Kolokythas K., Kantharia N. G., Raychaudhury S., David L. P., Vrtilek J. M., 2018a, MNRAS, 473, 5248
O'Sullivan E. et al., 2018b, A&A, 618A, 126
Panagoulia E. K., Fabian A. C., Sanders J. S., Hlavacek-Larrondo J., 2014, MNRAS, 444, 1236
Paturel G., Petit C., Prugniel P., Theureau G., Rousseau J., Brouty M., Dubois P., Cambrésy L., 2003, A&A, 412, 45
Rafferty D. A., McNamara B. R., Nulsen P. E. J., Wise M. W., 2006, ApJ, 652, 216
Sabater J. et al., 2019, A&A, 622, A17
Salim S. et al., 2007, ApJS, 173, 267
Scaife A. M. M., Heald G. H., 2012, MNRAS, 423, L30
Schweizer F., Seitzer P., Kelson D. D., Villanueva E. V., Walth G. L., 2013, ApJ, 773, 148
Shabala S. S., Ash S., Alexander P., Riley J. M., 2008, MNRAS, 388, 625
Sirothia S. K., Saikia D. J., Ishwara-Chandra C. H., Kantharia N. G., 2009, MNRAS, 392, 1403
Skibba R. A., Sheth R. K., 2009, MNRAS, 392, 1080
Smolčić V. et al., 2017, A&A, 602, A2
Stott J. P. et al., 2010, ApJ, 718, 23
Sun M., 2012, NJPh, 14d5004S
Sun M., Forman W., Vikhlinin A., Hornstrup A., Jones C., Murray S. S., 2003, ApJ, 598, 250
Taylor J. E., Babul A., 2005, MNRAS, 364, 515
Vaddi S., O'Dea C. P., Baum S. A., Whitmore S., Ahmed R., Pierce K., Leary S., 2016, ApJ, 818, 182
van den Bosch F. C., Jiang F., Hearin A., Campbell D., Watson D., Padmanabhan N., 2014, MNRAS, 445, 1713
Venturi T., Giovannini G., Feretti L., Comoretto G., Wehrle A. E., 1993, ApJ, 408, 81
Venturi T., Giacintucci S., Brunetti G., Cassano R., Bardelli S., Dallacasa D., Setti G., 2007, A&A, 463, 937
Venturi T., Giacintucci S., Dallacasa D., Cassano R., Brunetti G., Bardelli S., Setti G., 2008, A&A, 484, 327
Von Der Linden A., Best P. N., Kauffmann G., White S. D. M., 2007, MNRAS, 379, 867
Worrall D. M., Birkinshaw M., Laing R. A., Cotton W. D., Bridle A. H., 2007, MNRAS, 380, 2
Yuan Z. S., Han J. L., Wen Z. L., 2016, MNRAS, 460, 3669

SUPPORTING INFORMATION

Supplementary data are available at *MNRAS* online.

Appendix A. Information on individual groups.
Appendix B. GMRT radio continuum images.
Appendix C. BGE calculated properties for CLoGS sample.

Please note: Oxford University Press is not responsible for the content or functionality of any supporting materials supplied by the authors. Any queries (other than missing material) should be directed to the corresponding author for the article.

This paper has been typeset from a TEX/LATEX file prepared by the author.